MEASUREMENTS AND ANALYSIS OF ELECTRICAL INPUTS TO ADJUSTABLE SPEED MOTORS AND THEIR POWER ELECTRONIC CONVERTERS

By

DARIUSZ CZARKOWSKI

A DISSERTATION PRESENTED TO THE GRADUATE SCHOOL
OF THE UNIVERSITY OF FLORIDA IN PARTIAL FULFILLMENT
OF THE REQUIREMENTS FOR THE DEGREE OF
DOCTOR OF PHILOSOPHY

UNIVERSITY OF FLORIDA

1996

UNIVERSITY OF FLORIDA LIBRARIES

This work is dedicated to my Parents whose support means so much to me.

ACKNOWLEDGEMENTS

The author would like to thank his advisor, Dr. Alexander Domijan, Jr., for offering many constructive suggestions and evaluations. Dr. Domijan's guidance and support were invaluable.

The author wishes to express his gratitude to Dr. Thomas E. Bullock, Dr. Barney L. Capehart, Dr. Dennis P. Carroll, and Dr. Vladimir A. Rakov for their helpful suggestions and comments while serving on his committee.

Finally, the author would like to acknowledge the American Society of Heating, Refrigerating, and Air-conditioning Engineers (ASHRAE) for partial sponsorship of this work under Research Project 770. The wavelet analysis research was funded by the ASHRAE Grant-in-Aid to the author.

TABLE OF CONTENTS

ACKNOWLEDGEMENTS iii

LIST OF TABLES vi

LIST OF FIGURES vii

ABSTRACT ix

CHAPTERS

1 INTRODUCTION 1
1.1 Power Electronics and Power Quality 1
1.2 Metering Practices 4
1.3 Major Contributions 7
1.4 Organization of Dissertation 8

2 FFT ANALYSIS OF ASD WAVEFORMS 10
2.1 Waveforms 10
2.2 Recreation of Waveforms with FFT 18
2.2.1 Fast Fourier Transform 18
2.2.2 Recreation of Waveforms 20

3 PERFORMANCE OF POWER METERS IN ASD APPLICATIONS . . . 27
3.1 Meter Selection 27
3.2 Test Results 31
3.2.1 Real-World Conditions 31
3.2.2 Computer-Controlled Environment 33
3.2.3 Additional Tests 37
3.3 Meter Evaluation Criteria 37
3.4 Metering Implications of Waveforms Harmonic Content 43

4 TESTING PROCEDURES FOR ASD'S AND MOTORS 46
4.1 Equipment 46
4.1.1 Instrumentation 46
4.1.2 ASD's and Motors 50
4.2 Measurement Procedures 53
4.2.1 Squirrel Cage Induction Motor-ASD Set Testing Procedure 56
4.2.2 Brushless dc Motor-ASD Set Testing Procedure 59
4.2.3 Switched-Reluctance Motor-ASD Set Testing Procedure . 63

5 WAVELET TRANSFORM ANALYSIS OF ASD WAVEFORMS 68
5.1 Wavelet Transform versus FFT 68
5.2 Mother Wavelet Selection 73
5.3 Analysis of Waveforms with DWT 81

6 CONCLUSIONS 93
6.1 Summary and Conclusions 93
6.2 Suggestions for Further Research 95

REFERENCES 97

BIOGRAPHICAL SKETCH 100

LIST OF TABLES

2.1 Measured rms Values of ASD's Voltage and Current Waveforms. . . . 17

2.2 THD values of the Waveforms and Rms Values of Differences Between Recorded Waveforms and Waveforms Recreated with 50 Harmonics. . 21

3.1 Instruments for the Measurement of Non-Sinusoidal Power: Their Main Features. 29

3.2 Instruments for the Measurement of Non-Sinusoidal Power: Their Accuracy on Current, Voltage, and Power. 30

3.3 Converter Efficiencies at Full and 50% Load as Determined by Different Power Meters 33

3.4 Test Results for Meter_1 35

3.5 Test Results for Meter_2 36

3.6 Test Results for Meter_3 38

3.7 Test Results for Meter_2 at $V_{rms} = 125$ V, $I_{rms} = 15$ A, and $PF = 1$. 39

3.8 Test Results for Meter_2 at $V_{rms} = 125$ V and $I_{rms} = 15$ A. 40

4.1 Voltage and Current Transducer Manufacturers. Literature-Review Summary. 47

4.2 Nameplate Data of the Induction Motor Under Test. 56

4.3 Induction Motor-ASD Separation of Losses and Efficiencies 60

4.4 Induction Motor Separation of Losses 61

4.5 Brushless dc Motor-ASD Separation of Losses and Efficiencies 64

4.6 Switched-Reluctance Motor-ASD Separation of Losses and Efficiencies 67

5.1 Rms Values of Differences Between Recorded Waveforms and Waveforms Recreated with Various Mother Wavelets. 76

5.2 Rms Values of Differences Between Recorded Waveforms and Waveforms Recreated with 51 Components. 83

LIST OF FIGURES

1.1 Value of electric motors and drives in the U.S. factory automation market. 2

2.1 A block diagram of a PWM adjustable speed drive. 10

2.2 Normalized waveforms and their spectra at the input of the 3-phase rectifier. (a) Voltage and current waveforms. (b) Current spectrum. (c) Voltage spectrum. 12

2.3 Normalized waveforms and their spectra at the input of the induction motor. (a) Voltage and current waveforms. (b) Current spectrum. (c) Voltage spectrum. 13

2.4 Normalized waveforms and their spectra at the input of the 1-phase rectifier. (a) Voltage and current waveforms. (b) Current spectrum. (c) Voltage spectrum. 14

2.5 Normalized waveforms and their spectra at the input of the brushless-dc motor. (a) Voltage and current waveforms. (b) Current spectrum. (c) Voltage spectrum. 15

2.6 Normalized waveforms and their spectra at the input of the switched-reluctance motor. (a) Voltage and current waveforms. (b) Current spectrum. (c) Voltage spectrum. 16

2.7 Normalized PWM induction motor voltage waveform. (a) Recorded. (b) Recreated with first 50 harmonics. (c) Recreated with 50 most significant harmonics. 22

2.8 Normalized brushless-dc motor voltage waveform. (a) Recorded. (b) Recreated with first 50 harmonics. (c) Recreated with 50 most significant harmonics. 23

2.9 Normalized switched-reluctance motor voltage waveform. (a) Recorded. (b) Recreated with first 50 harmonics. (c) Recreated with 50 most significant harmonics. 24

2.10 Normalized brushless-dc motor current waveform. (a) Recorded. (b) Recreated with first 50 harmonics. (c) Recreated with 50 most significant harmonics. 26

4.1 An example of a suggested accuracy surface. 49

4.2 Schematic cross sections of motors. (a) Induction motor. (b) Brushless-dc motor. (c) Switched-reluctance motor. 52

4.3 PWM inverters. (a) For induction and brushless-dc motors. (b) For switched-reluctance motor. 54

5.1 Time-frequency plane coverages. (a) With the short-time Fourier transform. (b) With the wavelet transform. 70

5.2 Time-frequency plane coverages. (a) With the wavelet packet transform. (b) With the adapted general dyadic transform. 72

5.3 Wavelets of compact support with various degrees of smoothness . . 74

5.4 Induction motor voltage waveform recreated using Haar wavelet. . . 77

5.5 Induction motor voltage waveform recreated using D6 wavelet. . . . 78

5.6 Induction motor voltage waveform recreated using C3 Coiflet. 79

5.7 Induction motor voltage waveform recreated using S6 Symmlet. . . . 80

5.8 Induction motor current waveform recreated using S6 Symmlet. . . . 81

5.9 Switched-reluctance motor voltage waveform recreated using S6 Symmlet. 82

5.10 Switched-reluctance motor current waveform recreated with 51 DWT components. 84

5.11 Brushless-dc motor current waveform recreated with 51 DWT components. 85

5.12 Brushless-dc motor voltage waveform recreated with 51 DWT components. 86

5.13 Discrete wavelet transform analysis of induction motor voltage waveform. (a) S6 Symmlet coefficients. (b) Multi-resolution representation. 88

5.14 Discrete wavelet transform analysis of induction motor current waveform. (a) S6 Symmlet coefficients. (b) Multi-resolution representation. 89

5.15 Phase plane representation of the induction motor voltage waveform. 90

5.16 Phase plane representation of the brushless-dc motor voltage waveform. 91

5.17 Phase plane representation of the switched-reluctance motor voltage waveform. 92

Abstract of Dissertation Presented to the Graduate School
of the University of Florida in Partial Fulfillment of the
Requirements for the Degree of Doctor of Philosophy

MEASUREMENTS AND ANALYSIS OF ELECTRICAL INPUTS TO ADJUSTABLE SPEED MOTORS AND THEIR POWER ELECTRONIC CONVERTERS

By

Dariusz Czarkowski

August 1996

Chairman: Dr. Alexander Domijan, Jr.
Major Department: Electrical and Computer Engineering

This dissertation presents theoretical developments, results of laboratory experiments and tests, and digital signal analysis in the area of measurements and monitoring of voltage, current, and power waveforms that are characteristic for the three most common fractional and integral horsepower adjustable speed drive (ASD) technologies. The drive technologies under investigation are pulse-width modulated (PWM) induction, brushless-dc, and switched-reluctance drives.

Power electronic converters, which are at the heart of ASD's, shape current and voltage waveforms both at power-grid–ASD and ASD–motor terminals making the waveforms nonsinusoidal. Accurate measurements of electrical power under nonsinusoidal waveform conditions pose a twofold challenge for engineers and scientists, firstly, to select an instrument best suited to precisely measure and analyze a particular type of distortion, and, secondly, to correctly interpret the results. This work

gives frequency-domain analysis of recorded waveforms using the fast Fourier transform (FFT). The harmonic spectrum of PWM inverter-fed brushless-dc and switched-reluctance motors are presented for the first time. It is shown that the IEEE Std 519 recommended monitoring of the first 50 harmonics is sufficient for the ASD input voltages and currents. The analysis of switched voltages that are supplied by PWM inverters to the motors requires, however, consideration of several hundred components. Accuracy test results of three digital power meters subjected to ASD waveforms are presented. All meters failed to measure accurately powers at the input to the brushless-dc and to the switched-reluctance motor. Suggestions for improvement of the meters' performance are given. The present industry standards give testing methods for obtaining the energy efficiency of electric motors under pure sinusoidal or dc conditions. This work suggests procedures for energy efficiency testing and separation of losses in motor-ASD sets. To overcome Fourier transform drawbacks in analysis of PWM-type non-stationary waveforms, a new tool of the wavelet analysis is applied. Examples of time-frequency decomposition of ASD waveforms are shown. Conclusions and suggestions for further research are given.

CHAPTER 1
INTRODUCTION

1.1 Power Electronics and Power Quality

The beginning of power electronics can be traced back to 1958 when General Electric introduced the thyristor–the first solid-state power device. Many new and improved power devices have been developed since then: bipolar power transistors, gate-turn-off thyristors (GTO's), power metal-oxide semiconductor field-effect transistors (MOSFET's), insulated-gate bipolar transistors (IGBT's), and MOS-controlled thyristors (MCT's) to name the most important ones. Applications of power electronics cover areas ranging from hundreds of megawatts in high-voltage dc transmission (HVDC) systems to tens of watts in low-power switching power supplies and electronic ballasts. The operating frequency of power semiconductor devices ranges from tens to fractions of a hertz in HVDC and flexible ac transmission systems (FACTS) to megahertz in microwave ovens. Over the last two decades, power electronics has become an established and mature technology.

Advances in power electronics and control gave birth to a new field of technology related to the movement of objects. This field, called motion control, is deeply rooted in power electronics but has different objectives. In power electronics, the main goal is to efficiently transform electric energy. The goal of motion control is to change the position (servo systems) or speed of moving objects. Fig. 1.1 shows the value of all motor and drives for controlled position and speed applications in the U.S. factory automation sector in 1995 and as projected for the year 2000 [1]. A trend of an increasing market penetration of three-phase ac and brushless-dc and switched-reluctance motors at the expense of standard dc motors is observed.

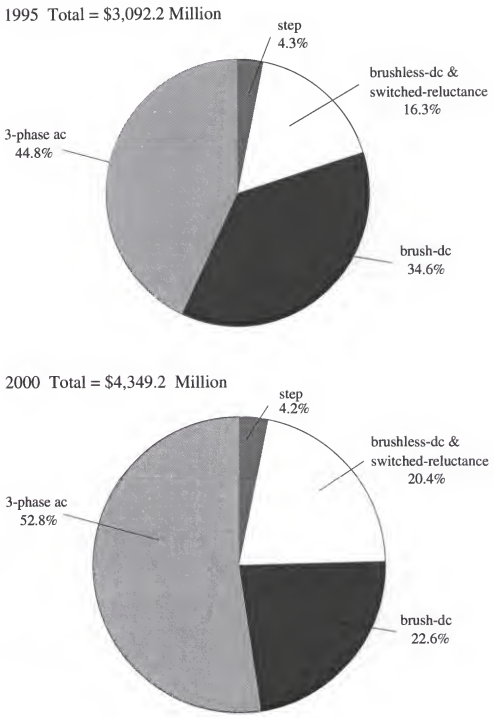

Figure 1.1: Value of electric motors and drives in the U.S. factory automation market.

The cross section of power electronics and motion control is very important economically in the area of adjustable speed drives (ASD's). ASD's need to provide control of the rotating speed of electrical machinery while maintaining at the same time high efficiency of energy transformation from electrical to mechanical. The most common type of ASD's use a pulse-width modulated (PWM) inverter. The utility voltage is rectified to an approximately constant magnitude or a dc voltage is obtained from a battery in the case of, for instance, electric vehicles. The dc voltage is then transformed to ac using switching devices. The required sinusoidal or trapezoidal shape of currents in motor windings is achieved by varying the duty ratio, that is, the time-on to time-on plus time-off ratio of semiconductor power switches.

The dramatic increase in power electronic equipment applications has caused difficulties associated with electric power quality. This term refers to maintaining a desired shape, usually sinusoidal, trapezoidal, or constant, of voltage and current waveforms at rated voltage or current magnitude and frequency in the case of alternating signals. Adjustable speed drives affect power quality on both the utility side and the motor side [2]-[6]. The nonlinear switching action of power semiconductor devices produces current and voltage waveforms with rich harmonic spectra. At the power-grid side, it is the discontinuously drawn by the rectifier current that has a high harmonic content. At the motor side, the switched dc voltage has a very high harmonic content by the principle of the PWM action. Motor currents are smoothed by inductances of the motor windings and their harmonic content is lower than that of the voltage. Monitoring of harmonics at the power-grid side is needed to comply with the guidelines of the IEEE Std 519 [7]. Harmonic analysis of the motor waveforms helps in designing more efficient and reliable drives and in limiting electromagnetic interference (EMI) that may affect operation of other electronic equipment. Quasi steady-state power quality disturbances are most often analyzed using methods based

on Fourier series, predominantly the fast Fourier transform (FFT) and its modifications. However, the underlying periodicity assumption for use of the FFT is not very well satisfied in today's dynamic electric environment. Transient power quality disturbances are monitored and analyzed in time domain or using emerging wavelet transform domain methods.

1.2 Metering Practices

Measurements of electrical quantities of distorted waveforms that are being produced by ASD's and other power electronic equipment pose a serious challenge for engineers and scientists. There are two kinds of problems associated with power measurements. One is to select an instrument best suited to precisely measure under a particular type of distortion, the other is to interpret correctly the results. Accurate power measurement under nonsinusoidal conditions carries valuable information for designers, manufacturers, and users of ASD's. Firstly, it makes it possible to determine the efficiency of the drive. Secondly, it allows for separation of losses between a power electronic part and a motor which is needed to optimize the efficiency performance of the whole unit. Knowledge of harmonic content of distorted waveforms is important for determining the accuracy of the measurement [8]. For modern power meters, the accuracy of voltage and current rms value measurements that reaches 0.05% at frequencies close to the fundamental (so called basic accuracy), decreases with an increase in frequency. Harmonic content is important for investigation of the behavior of various electric power apparatus. Harmonic level serves also as an index for electric equipment derating.

Since power generation and distribution systems are intended to supply a nearly sinusoidal voltage and current, the majority of electrical measuring equipment has been developed to operate accurately under balanced sinusoidal conditions. This

type of equipment, which usually uses analog transducers, e.g., induction wattmeters and watthour meters, does not provide accurate measurements under distorted current or voltage waveforms.

Power measurement accuracy of other types of meters under distorted [9], [10] and unbalanced [11] conditions has been studied. The time-division multiplier (TDM) meter produces an impulse whose amplitude is proportional to one input and width is proportional to the second input. Hence, the area of the impulse is proportional to the instantaneous product of both inputs (instant power when voltage and current are the inputs). The TDM wattmeters are widely used for 60 Hz power measurements. The frequency band of this type of meter is limited by the carrier frequency. There are commercial units available rated up to 20 kHz and prototypes with a carrier frequency of 500 kHz have been reported. A thermal wattmeter operates using a quarter-square-multiplier principle:

$$P = \frac{1}{T}\int_0^T v(t)i(t)dt = \frac{1}{4T}\{\int_0^T [v(t)+i(t)]dt\}^2 - \frac{1}{4T}\{\int_0^T [v(t)-i(t)]dt\}^2. \tag{1.1}$$

Thermal converters with a quadratic response are used to calculate the squares of the sum and difference of input waveforms. High accuracy standard wattmeters can be built using this technique. However, this technique is not very promising for bench and field instruments. The idea of a translinear (transconductance) multiplier (TLM) wattmeter is presented in [9] along with test results for a prototype. The accuracy of TLM meters depends mainly upon the accuracy of the integrated circuit which performs the multiplication function. Those integrated circuits have an excellent frequency response with a bandwidth in the 1 MHz range. However, their temperature coefficient is substantial. The most popular power meters and analyzers for nonsinusoidal applications are digital solid-state instruments. They calculate rms values, power, and energy from digital samples of current and voltage waveforms. Certain

types of digital solid-state meters were found to be well suited for power system applications. There were, however, no independent reports on the behavior of those meters when subjected to PWM types of waveforms that are produced by ASD's.

Besides accuracy, there is another problem that prevents a full utilization of digital sampling instruments in distorted waveform metering. It is an absence of standard and physically meaningful definitions for reactive power and for polyphase apparent power under distorted conditions [12]. The active power is defined as

$$P = \sum_n V_n I_n cos\phi_n \tag{1.2}$$

where V_n and I_n are the rms values of the voltage and current, respectively, and ϕ_n is the phase angle for the n-th harmonic component. The definition of active power causes no controversies. On the other hand, there is a plethora of reactive power definitions [13], [14], e.g., first harmonic reactive power, Budeanu's reactive power, Shepherd-Zakikhani's reactive power, Kusters-Moore's reactive power, Czarnecki's reactive power, Kimbark's reactive power, Depenbrock's reactive power, Enslin and Van Wyk's reactive power, and Sharon's reactive power. Modern digital power meters calculate so called Fryze's reactive power which is based on the current being split into active and reactive currents

$$i = i_a + i_r. \tag{1.3}$$

The reactive current is the "useless" component which does not contribute to the net energy transfer. The active, reactive, and apparent power are defined in terms of the rms values of currents i_a and i_r, and the rms voltage V

$$Q_F = VI_r = \sqrt{(VI)^2 - (VI_a)^2} = \sqrt{S^2 - P^2} \tag{1.4}$$

where S denotes the apparent power. For the polyphase apparent power, the main controversy is if the system should be considered as a whole or as a sum of separate

phases [15]. In a "phase-by-phase" approach, the apparent power of the system is

$$S_A = \sum_k V_k I_k. \tag{1.5}$$

If the system is considered as a whole, the system apparent power is

$$S_{SYS} = \sqrt{\sum_k I_k^2} \sqrt{\sum_k V_k^2}. \tag{1.6}$$

Since $S_A \leq S_{SYS}$, compensation based on S_{SYS} allows for more efficient use of the power system.

1.3 Major Contributions

Major contributions of this dissertation to the field of measurement and analysis of electrical signals and to related areas are itemized below.

- Harmonic analysis has been conducted for waveforms that were recorded for the three main adjustable speed drive technologies, namely, induction, brushless-dc, and switched-reluctance drives. For the first time harmonic content of electric inputs to PWM inverter-fed brushless-dc and switched-reluctance motors is presented. The IEEE Std 519 suggested practices for harmonic monitoring are critically evaluated.

- Power and rms value accuracy tests have been performed on three modern digital power meters. The tests have been conducted using both real-world waveforms and waveforms reproduced in a computer-controlled environment. Suggestions for the improvement of meter performance are presented.

- Testing procedures for ASD-motor sets have been proposed. The procedures may form the basis for development of future standards in this area.

- A wavelet transform technique has been introduced to the field of ASD waveform analysis. This technique overcomes many pitfalls of the presently used Fourier transform.

1.4 Organization of Dissertation

This dissertation is composed of six chapters. They present theoretical developments, results of laboratory experiments and tests, and digital signal analysis in the area of measurements and monitoring of adjustable speed drive waveforms.

Chapter 1 contains a brief overview of the state-of-the-art in the power electronics and measurement areas as related to adjustable speed drives. Challenging problems for scientists and engineers are pointed out. Major contributions of this work are listed. The fast Fourier transform analysis of waveforms recorded for the three main ASD technologies, namely, PWM induction, brushless-dc, and switched-reluctance drives, is presented in Chapter 2. This classical approach to the frequency-domain analysis is critically evaluated based on the IEEE Std 519 recommended practices. Chapter 2 gives a thorough characterization of waveforms that are used for meter testing of Chapter 3. Chapter 3 gives results of accuracy tests of three modern digital power meters and analyzers. The meters were tested under real-world and computer controlled conditions. Sources of measurement errors are addressed and suggestions for meters' performance improvements are given. Chapter 4 contains test procedures for ASD-motor sets. The proposed tests lead to evaluation of efficiencies and to separation of losses between an ASD and a motor and in the motor itself. This chapter also discusses test instrumentation and design features of ASD's and motors that affect test procedures. A new method of distorted ASD waveform analysis is introduced in Chapter 5. This method is based on the wavelet transform which provides time-frequency information of the analyzed signal. Results of analysis of

recorded PWM type waveforms are presented and compared to the FFT analysis. A summary of this dissertation results, conclusions, and suggestions for further research are given in Chapter 6.

CHAPTER 2
FFT ANALYSIS OF ASD WAVEFORMS

2.1 Waveforms

The past two decades have witnessed a proliferation of adjustable speed drives (ASD's) due to the energy savings and versatility of operation that they offer. As schematically shown in Fig. 2.1, a typical fractional or integral horsepower ASD is built from three basic blocks: a peak rectifier connected to the power grid, a dc link, and a PWM type inverter at the motor side. The nonlinear switching action of power semiconductor devices produces current and voltage waveforms with rich harmonic spectra [18]. At the power-grid side, it is the discontinuously drawn by the rectifier current that has a high harmonic content. At the motor side, the switched dc voltage has a very high harmonic content by the principle of the PWM action. Motor currents are smoothed by inductances of the motor windings and their harmonic content is lower than that of the voltage. Monitoring of harmonics at the power-grid side is needed to comply with the guidelines of the IEEE Std 519 [7]. Harmonic

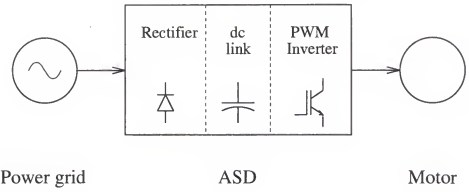

Figure 2.1: A block diagram of a PWM adjustable speed drive.

analysis of the motor waveforms helps in designing more efficient and reliable drives and in limiting electromagnetic interference (EMI) that may affect operation of other electronic equipment.

The tested meters were subjected to a variety of current and voltage waveforms that can occur in ASD applications, particularly in HVAC equipment. Waveforms that are characteristic for three main drive technologies used in adjustable speed air conditioners and heat pumps were investigated. These technologies are PWM induction drive, brushless-dc drive, and switched-reluctance drive. The PWM induction drive was a 230 V 3-phase device. It was loaded by a 5 hp 3-phase induction motor. The rated speed of the motor was 1750 rpm at full load. The brushless-dc drive was a 120 V single-phase unit. It was driving a 1 hp 3-phase motor. The full load was applied to the motor at 1100 rpm. The switched-reluctance drive was a 230 V single-phase device. It was combined with a 1/3 hp 4-phase motor that was loaded by a blower. The full load was at 1200 rpm of the motor.

The normalized with respect to peak values voltage and current waveforms and their spectra for a 3-phase PWM induction drive operating at a speed of 1800 rpm are shown in Figs. 2.2 and 2.3. The input of the drive is a 3-phase rectifier. It can be seen in Fig. 2.2 that the input voltage to the rectifier is practically sinusoidal. The pulsating input current is rich in odd harmonics, especially 5th, 7th, 11th, 13th, 17th, and 19th. However, for both input voltage and current, the Fourier analysis up to 50 harmonics is sufficient. The output of the drive is a 3-phase PWM inverter whose normalized phase voltage and current waveforms are depicted in Fig. 2.3. The spectrum of the switched rectangular voltage extends beyond 50 harmonics.

A single-phase rectifier is the input for both brushless-dc and switched-reluctance drives. Fig. 2.4 shows normalized voltage and current waveforms and their spectra for the rectifier. The voltage waveform is a sinusoid. The current waveform has a high content of odd harmonics up to around 40. The magnitudes of current harmonics 3

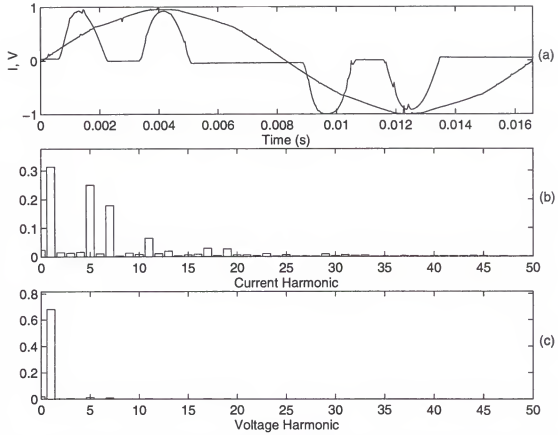

Figure 2.2: Normalized waveforms and their spectra at the input of the 3-phase rectifier. (a) Voltage and current waveforms. (b) Current spectrum. (c) Voltage spectrum.

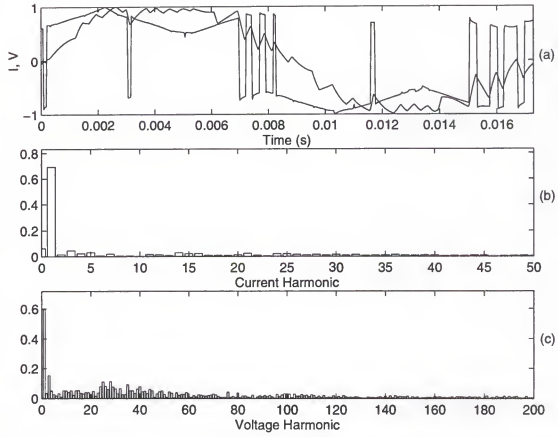

Figure 2.3: Normalized waveforms and their spectra at the input of the induction motor. (a) Voltage and current waveforms. (b) Current spectrum. (c) Voltage spectrum.

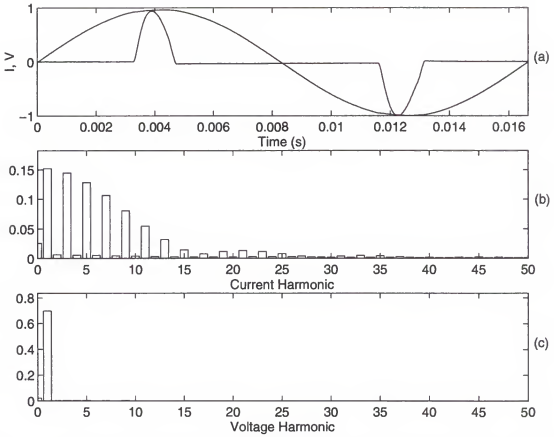

Figure 2.4: Normalized waveforms and their spectra at the input of the 1-phase rectifier. (a) Voltage and current waveforms. (b) Current spectrum. (c) Voltage spectrum.

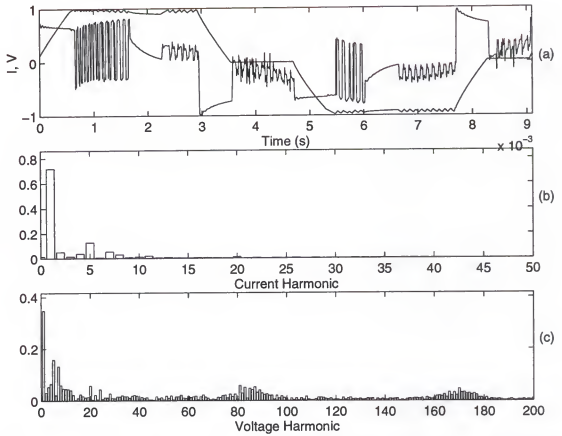

Figure 2.5: Normalized waveforms and their spectra at the input of the brushless-dc motor. (a) Voltage and current waveforms. (b) Current spectrum. (c) Voltage spectrum.

through 17 slowly decrease with the 3rd harmonic almost as high as the fundamental component.

Fig. 2.5 shows normalized voltage and current waveforms and their spectra at the input to a 3-phase brushless-dc motor operating at 1100 rpm. It can be seen that the voltage harmonic spectrum extends beyond 200 harmonics. This is due to the high-frequency PWM action of the converter. The highest significant current harmonic is 20.

The normalized voltage and current waveforms and their spectra at the input to a 4-phase switched-reluctance motor operating at 1200 rpm are depicted in Fig. 2.6. A significant peak of harmonics can be observed in the rich voltage harmonic spectrum. It indicates that a constant PWM switching frequency of about

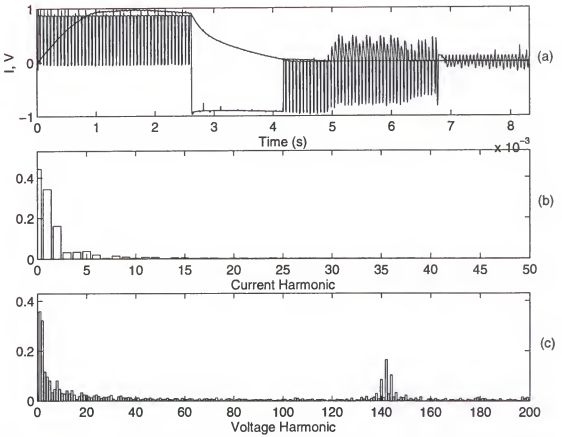

Figure 2.6: Normalized waveforms and their spectra at the input of the switched-reluctance motor. (a) Voltage and current waveforms. (b) Current spectrum. (c) Voltage spectrum.

17 kHz is employed in the converter. The current harmonic spectrum extends only to 20 harmonics. Note, however, that the dc component is dominant in the current waveform.

The waveforms presented in this section for multi-phase devices are given for one phase only because the shape for other phases is identical. The waveforms have been normalized with respect to its peak values to facilitate a comparison between particular harmonic contents. For instance, it could be observed that the fundamental component of the 3-phase rectifier current is about two times higher than the fundamental component of the 1-phase rectifier current. The measured rms values of the waveforms presented in Figs. 2.2–2.6 are given in Table 2.1. The values of the 1-phase rectifier waveforms are given for both the switched-reluctance drive and the brushless-dc drive.

Table 2.1: Measured rms Values of ASD's Voltage and Current Waveforms.

Waveform Type	rms values	
	Voltage (V)	Current (A)
3-phase rectifier	132.1	18.30
Induction motor	244.0	15.13
1-phase rectifier switched-reluctance drive	227.3	2.90
1-phase rectifier Brushless-dc drive	119.4	12.24
brushless-dc motor	213.6	8.07
Switched-reluctance motor	215.9	1.01

2.2 Recreation of Waveforms with FFT

2.2.1 Fast Fourier Transform

According to Fourier analysis, the values of the time domain signal $x(t)$ sampled N times per period can be expressed as

$$x(t_n) = \sum_{k=0}^{N-1} X(f_k) e^{j2\pi kn/N} \tag{2.1}$$

where

$$X(f_k) = \frac{1}{N} \sum_{n=0}^{N-1} x(t_n) e^{-j2\pi kn/N}. \tag{2.2}$$

A fast procedure for calculating coefficients $X(f_k)$ of a uniformly sampled signal is known as the fast Fourier transform (FFT). To speed up the calculation process, the FFT algorithm takes advantage of the periodic character of terms $e^{-j2\pi kn/N}$ and uses so called 'butterfly' matrix computational techniques [16]. This name has its origin in a graphical representation of the FFT flow chart where computation of each coefficient $X(f_k)$ reminds one of the flight of a butterfly. The 'butterfly' operations are performed by dedicated integrated circuits.

Application of instruments that use the FFT for signal processing without understanding the limitations of this method may lead to erroneous results. The FFT method assumes that the analyzed waveforms are periodic and stationary, the sampling interval must be exactly an integer multiple of a waveform period, and the waveform does not contain so called "non-integer harmonics", that is, components with frequencies that are not integer multiples of the fundamental frequency. Obviously, the Nyquist sampling criterion must also be satisfied. The Nyquist criterion states that the sampling frequency should be at least twice the highest harmonic frequency of the signal. However, to obtain accurate results with a not very long sampling interval, it is usually suggested in practice that the sampling frequency be

about 10 times the highest harmonic frequency. Three major pitfalls associated with the FFT can be distinguished [17]: aliasing, picket-fence effect, and leakage.

Aliasing

Aliasing occurs when high frequency harmonics of the signal are translated by FFT into low frequency components. This problem can be alleviated by increasing the sampling frequency. However, even when the Nyquist criterion is satisfied, aliasing may still occur. In this case, it is referred to as "pseudoaliasing". Harmonic analyzers are equipped with low-pass antialiasing filters. However, the less than ideal nature of those filters can cause distortions of the measured signal. Another antialiasing technique is comparing the measurement results at different sampling frequencies. This solution adds greatly to the complexity of meters.

Picket-Fence Effect

The picket-fence effect takes place when the analyzed waveform contains frequency components that are not integer multiples of the fundamental frequency. Such "non-integer harmonics" may remain unrecognized by a meter or their contribution to the power transfer may be erroneously accounted for. Non-integer harmonics are present when a motor-drive system is not completely in its steady state. There were also reports on a presence of substantial non-integer harmonics in the steady-state of, for instance, a synchronous motor supplied from a load commutated six-pulse inverter.

Leakage

The leakage effect describes the apparent spreading of energy from one frequency to adjacent ones. It occurs when the sampling interval is not exactly an integer multiple of a waveform period. In reality, the frequency of the fundamental component has some fluctuations that cause a truncation of the signal not exactly at the end of a cycle when the sampling interval is set constant based on the expected

value of the fundamental frequency. Leakage is reduced by applying window techniques, that is, multiplying the analyzed waveform by an appropriate time domain function. There is, however, no optimum window shape for all applications.

2.2.2 Recreation of Waveforms

The IEEE Std 519 defines verbally the total harmonic distortion (THD) ([7] p. 11) as

$$THD = \sqrt{\frac{\text{sum of squares of amplitudes of all harmonics}}{\text{square of amplitude of fundamental}}} \times 100\%. \tag{2.3}$$

However, this definition applied to the power system voltage on page 63 is given as

$$THD = \frac{\sqrt{\sum_{h=2}^{50} V_h^2}}{V_1} \times 100\%. \tag{2.4}$$

Also, the required 3 kHz bandwidth of instruments for power system harmonic measurements, as specified on page 68, suggests that monitoring the first 50 harmonics is sufficient. This recommendation has been adopted by precision power meter and analyzer manufacturers whose products perform FFT analysis of measured waveforms up to 50 or, in some cases, up to 99 harmonics. At the power grid side, the meters provide THD information accurately. However, monitoring of the first 50 or even first 100 harmonics is not sufficient for the voltage and current waveforms supplied to motors by PWM inverter type ASD's.

Rich harmonic spectra of, especially, voltage waveforms of the motors could be observed in Figs. 2.3, 2.5, and 2.6. The voltage spectra extend beyond the first 50 harmonics. The effects of taking into account only 50 harmonics in recreation of recorded waveforms were investigated numerically. Table 2.2 shows THD's of the waveforms of Figs. 2.2–2.6, THD's of the recreated waveforms and errors of recreation using the first 50 and 50 most significant harmonics, respectively. The most significant harmonics were selected according to the magnitude of components. The dc

Table 2.2: THD values of the Waveforms and Rms Values of Differences Between Recorded Waveforms and Waveforms Recreated with 50 Harmonics.

Waveform Type		Recorded	Recreated with 50 Harmonics			
			First		Most Significant	
		THD (%)	THD (%)	Error	THD (%)	Error
3-phase	V	2.62	2.39	0.0269	2.44	0.0274
rectifier	I	102.21	102.15	0.0437	102.15	0.0439
Induction	V	74.23	65.56	0.2403	67.26	0.2381
motor	I	15.02	14.90	0.0270	14.91	0.0269
1-phase	V	0.74	0.73	0.0308	0.73	0.0308
rectifier	I	161.56	161.54	0.0408	161.54	0.0407
brushless-dc	V	103.86	78.24	0.2399	92.08	0.2292
motor	I	21.84	21.81	0.0120	21.83	0.0105
SR	V	142.03	111.47	0.3155	135.58	0.2464
motor	I	50.99	50.97	0.0052	50.98	0.0046

component was added regardless of its magnitude. The error of recreation is defined as the rms value of the difference between recorded and recreated waveforms

$$E_r = \sqrt{\frac{1}{T}\int_0^T [f(t) - f_r(t)]^2 dt} \tag{2.5}$$

or, in a discrete version,

$$E_r = \sqrt{\frac{1}{N}\sum_{k=1}^{N} [f(k) - f_r(k)]^2} \tag{2.6}$$

where f is the recorded waveform, f_r is the recreated waveform, T is the recording time, and N is the number of samples.

It could be seen in Table 2.2 that the highest recreation errors were, as expected, for the motors' voltage waveforms. Figs. 2.7–2.9 show the recorded and recreated voltage waveforms for the induction, brushless-dc, and switched-reluctance motor, respectively. In the case of PWM induction drive, both types of recreation with 50 harmonics, shown in Fig. 2.7(b) and (c), failed to show sharp edges of the rectangular PWM voltage. In the case of brushless-dc and switched-reluctance

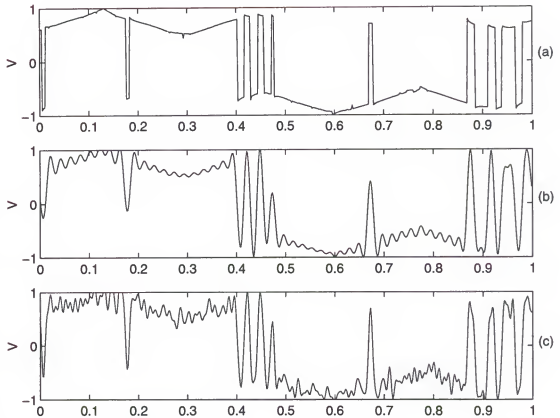

Figure 2.7: Normalized PWM induction motor voltage waveform. (a) Recorded. (b) Recreated with first 50 harmonics. (c) Recreated with 50 most significant harmonics.

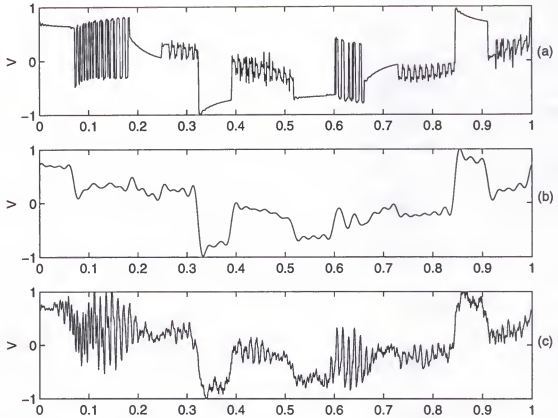

Figure 2.8: Normalized brushless-dc motor voltage waveform. (a) Recorded. (b) Recreated with first 50 harmonics. (c) Recreated with 50 most significant harmonics.

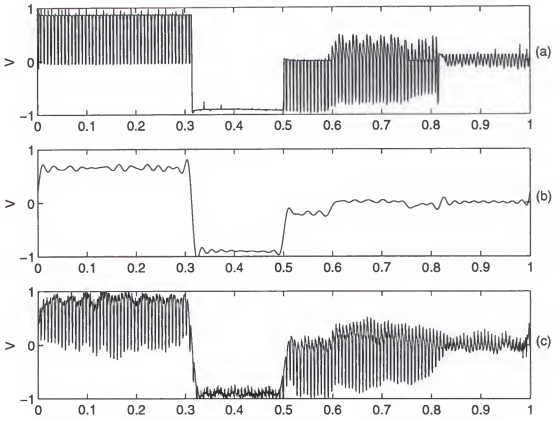

Figure 2.9: Normalized switched-reluctance motor voltage waveform. (a) Recorded. (b) Recreated with first 50 harmonics. (c) Recreated with 50 most significant harmonics.

drives, the recreation with the first 50 harmonics does not show PWM switching action at all (see Figs. 2.8(b) and 2.9(b)). Among the 50 most significant harmonics for the brushless-dc motor voltage waveform, there are 17 components of the 57-96 harmonic group, 13 components of the 164-177 harmonic group, and 340th and 344th harmonics. The rest of the most significant components is of the order below 50. For the switched-reluctance motor, there are 9 components of the 134-156 harmonic group, 8 components of the 276-288 group, 4 components of the 424-428 group, and 710th, 852th, and 994th harmonics. Although the recreation with 50 most significant harmonics shows the presence of the high-frequency PWM switching as depicted in Figs. 2.8(c) and 2.9(c), the error of recreation defined by (2.6) still remains high. The recreation error for current waveforms is low. An example of a recorded and recreated current waveform for the brushless-dc motor is shown in Fig. 2.10.

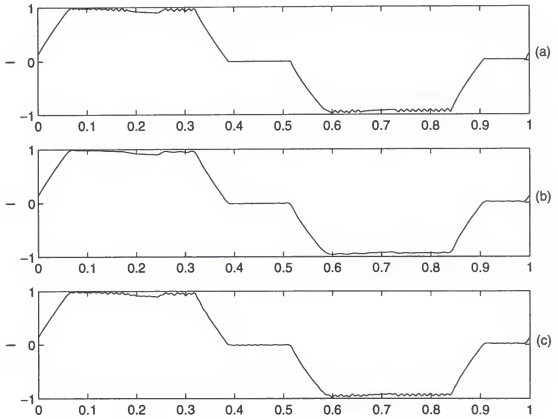

Figure 2.10: Normalized brushless-dc motor current waveform. (a) Recorded. (b) Recreated with first 50 harmonics. (c) Recreated with 50 most significant harmonics.

CHAPTER 3
PERFORMANCE OF POWER METERS IN ASD APPLICATIONS

3.1 Meter Selection

Modern power meters and analyzers are digital solid-state instruments that are equipped with microprocessors. The measured current and voltage waveforms are sampled at a frequency of the order of 100 kHz. The samples are converted to a digital representation with A/D converters and stored in an internal memory. The stored information is processed by digital signal processing (DSP) integrated circuits and displayed, printed out, or sent to external devices. DSP circuits can perform a great variety of mathematical operations that allows for obtaining characteristic parameters of acquired voltages and currents. The parameters that are usually extracted from the acquired waveforms include rms and mean values of voltage and current, real power, reactive power, apparent power, power factor, true power factor, voltage and current crest factor, frequency, peak current and voltage, peak inrush current, and many more. Units equipped with an integrator function display energy consumption, maximum demand, reactive energy consumption, and current consumption.

The distorted, that is nonsinusoidal, waveforms that the meters are subjected to are characterized in the frequency domain. According to the IEEE Std 519 [7], the meters should be able to calculate at least 50 harmonics of the fundamental frequency. Certain new models calculate up to 100 harmonics. Knowledge of harmonic content is essential for determining the accuracy of the measurement [19]. The accuracy that reaches 0.05% at frequencies close to the fundamental (so called basic accuracy), decreases with an increase in frequency. The important topic of frequency domain decomposition has been discussed in the previous chapter.

Modern power meters are equipped with a number of analog and digital inputs and outputs. For instance, analog inputs from torque and speed transducers are used for determining a motor or a drive efficiency. Analog outputs allow for displaying measured waveforms on an external oscilloscope. Data can be digitally sent to an external printer or computer. Finally, a power analyzer can be remotely controlled through digital inputs. Digital inputs and outputs are standardized as a serial RS-232 port, parallel and Centronics ports, and GPIB terminal.

After contacting manufacturers and reviewing obtained literature, Table 3.1 was created that presents the main features of the best power meters and analyzers available on the market. The basic accuracy for current, voltage, and power measurements of the instruments of Table 3.1 is given in Table 3.2.

Three meters, each from a different manufacturer, were obtained for a loan and laboratory tested [20]. They will be called Meter_1, Meter_2, and Meter_3.

Meter_1 was a several years old design which is presently considered the workhorse in the industry. Since introducing Meter_1 to the market, the manufacturer released its improved version with increased accuracy and special synchronization features for ASD's. The basic accuracy of Meter_1 is specified as 0.1% of reading + 0.05% of range for both voltage and current and 0.2% of reading + 0.15% of range for power. The bandwidth is dc and 0.1 Hz–200 kHz. Harmonic analysis is performed up to 50 components using the discrete Fourier algorithm. The maximum sampling frequency for the 3-phase configuration is 95 kHz.

Meter_2 was claimed by its manufacturer to have a unique operating principle that allows for the basic accuracy 0.03% of reading + 0.05% of range for voltage and current and 0.05% of reading + 0.05% of range for power. The measurement bandwidth is dc and 2 Hz–200 kHz. 50 harmonic components are calculated using an 8192 point fast Fourier transform. The maximum sampling frequency is 104 kHz.

Table 3.1: Instruments for the Measurement of Non-Sinusoidal Power: Their Main Features.

Brand Name	Φ	Mod. #	Input Specifications					Measurements																
			V(V)		I(A)		Freq.	Basic	Advanced														Harmonic	Other
			rms	peak	rms	peak	dc→kHz	a→d	e	f	g	h	i	j	k	l	m	n	o	p	q	r	s	t	u v w x	$\alpha\,\beta\,\gamma\,\delta$
Voltech	3	PM3300	1400	2000	30	200	500	●	●●●			●●●			●●●			●●●			●●●			●	●●●●	●●●●
	3	PM3000	1000	2000	30	200	200	●	●●●			●●●			●●●			●●●			●●●			●	●●●●	●●●●
	3	PM300	-	1000	16	200	250	●	●●●			●●●			●○○			●●○			○○○			○	●●●●	●○○●
Infratek	3	304B	1000	1400	20	-	100	●	●●●			○○○			○●●			○○●			●○○			○	○○○○	●○○○
	1	104B	1000	1400	20	-	200	●	○○○			○○○			○○○			○○○			○○○			○	○○○○	●○○○
	1	105A	700	-	25	-	20	●	●○○			○○○			○○○			○○○			●○○			○	○○○○	●○○○
Yokogawa	3	2533	600	1400	20	70	20	●	●●●			○○○			○●●			○○○			●○○			●	○○○○	●●○○
	3	2531	600	1000	35	250	200	●	●●●			●●●			●●●			●●●			●●●			●	●●●●	●●●●
Norma	6	D6100	1500	2100	1000	-	1000	●	●●●			●●●			●●●			●●●			●●●			●	●●●●	●●●●

NOTES:
- = information not available at time of printing
a. Vrms = true RMS voltage
b. Irms = true RMS current
c. PF = W/sqrt(W2+ VAR2)
d. True PF = W/Vrms*Irms
e. W = real power
f. VA = apparent power
g. VAR = reactive power
h. Vcf = voltage crest factor
i. Icf = current crest factor
j. Irush = peak inrush current
k. F = input frequency
l. Vmean = mean voltage
m. Imean = mean current
n. Vpk = peak voltage
o. Ipk = peak voltage
p. ZL = load impedance
q. W-hrs = energy consumption
r. VA-hrs = maximum demand
s. VAR-hrs = reactive energy consumed
t. I-hrs = amperes consumed
u. Vthd = THD for voltage
v. Ithd = THD for current
w. Vh = mag. + phase of harmonic V
x. Ih = mag. + phase of harmonic I

α. GPIB interface
β . Scaling
γ. Data logging up to few seconds
δ. Data dump to a printer

Table 3.2: Instruments for the Measurement of Non-Sinusoidal Power: Their Accuracy on Current, Voltage, and Power.

#	Company Name & Model No.	Freq. Range (Hz)	Current			Voltage			Power		
			Max.	Accuracy	Freq.(Hz)	Max.	Accuracy	Freq.(Hz)	Max.	Accuracy	Freq.(Hz)
1	Voltech PM3300	dc-1M	30A	0.05%rdg+ 0.05%range	45-450	2000V	0.05%rdg+ 0.05%range	45-450	400kW	0.15%rdg+ 0.1%range	45-450
2	Voltech PM3000	dc-200k	30A	0.1%rdg+ 0.05%range	45-450	1000V	0.1%rdg+ 0.05%range	45-450	400kW	0.2%rdg+ 0.15%range	45-450
3	Voltech PM300	dc-250k	16A	0.2%rdg+ 1mA	5-1k	1000V	0.2%rdg+ 10mV	5-1k	-	(0.4/PF)%rdg +2mW	5-1k
4	Infratek 104B	dc-200k	20A	0.1%rdg+ 0.1%range	40-1k	1000V	0.1%rdg+ 0.1%range	40-1k	20kW	0.1%rdg+ 0.1%range	40-400
5	Infratek 304B	dc-100k	150A	0.1%rdg+ 0.1%range	40-1k	1000V	0.1%rdg+ 0.1%range	40-1k	60kW	0.1%rdg+ 0.1%range	40-400
6	Infratek 105A	dc-20k	25A	0.2%rdg+ 0.25%range	15-5k	700V	0.2%rdg+ 0.25%range	15-5k	12kW	0.2%rdg+ 0.3%range	15-5k
7	Yokogawa 2533	dc-20k	20A	0.2%rdg+ 0.2%range	66-2k	600V	0.2%rdg+ 0.2%range	66-2k	-	0.2%rdg+ 0.2%range	66-2k
8	Yokogawa 2531	dc-200k	35A	0.03%rdg+ 0.05%range	30-1k	1000V	0.03%rdg+ 0.05%range	30-1k	-	0.05%rdg+ 0.05%range	30-1k
9	Norma D6100	dc-1M	1000A	0.09%rdg+ 0.05%range	45-65	2100V	0.09%rdg+ 0.02%range	45-65	-	0.2%rdg	50
10	Xitron 2503AH	dc-500k	50A	0.05%rdg+ 0.05%range	40-400	3000V	0.05%rdg+ 0.05%range	40-400	-	0.1%rdg+ 0.1%range	40-400

The basic accuracy of Meter_3 is specified as 0.09% of reading + 0.02% of range for voltage and 0.09% of reading + 0.05% of range for current. The accuracy of power measurements is given as a series of graphs for different values of frequency and power factor. The measurement bandwidth is dc–400 kHz. Up to 99 harmonics are calculated using the discrete Fourier transform. The maximum sampling frequency is 70 kHz.

A multichannel PC-based data acquisition system [21] was used as a reference meter. The system offers simultaneous data sampling with frequencies up to 1 MHz. The sampling frequency selected for all of the tests was 250 kHz. Voltage measurement channels were calibrated using a 5790A AC Measurement Standard by Fluke Corporation with a relative uncertainty of less than 35 parts per million at 60 Hz. Current measurement channels were calibrated using the ac measurement standard and a Fluke Y5020 Current Shunt of 0.025% accuracy. Since each current and voltage recording was calibrated with the ac measurement standard, the accuracy of the reference meter was affected mainly by its vertical resolution and rms noise. This accuracy is estimated to be 0.05% of the range for both voltage and current measurements and 0.1% of the range for power measurements.

3.2 Test Results

3.2.1 Real-World Conditions

The goal of this part of the experiment was to measure efficiencies of three different types of ASD's with the three tested meters and compare them to the efficiency obtained with the reference meter. The efficiency of each type of ASD was measured under full rated load and 50% load of their respective motors. The advantage of this test approach is that the meters are tested in similar conditions that they are operated in industrial laboratories or in the field. The disadvantage is that the real-world

waveforms are in a *quasi* steady-state. That is, the measured values of the voltage, current, and power oscillate around equilibrium points. For instance, it was measured that those oscillations can amount to 6% of the equilibrium value during a time span of twenty periods for the current waveform in the switched-reluctance motor. Since it was impossible to synchronize all the meters and set the same averaging period, the oscillations caused additional error in the efficiency measurements. The efficiencies of the drives were determined using the formula

$$Efficiency(\%) = \frac{Motor\ Input\ Power}{ASD\ Input\ Power} \times 100. \tag{3.1}$$

During the tests, all the meters had their respective voltage terminals connected in parallel and current terminals in series so they measured the same quantities. The switched-reluctance drive was a 230 V single-phase device. It was combined with a 1/3 hp 4-phase motor that was loaded by a blower. The full load was at 1200 rpm of the motor and the 50% load was at 900 rpm. Since the tested meters were all 3-phase meters, the input power and the power of 2 phases of the motor were measured. The power obtained for the motor was multiplied by 2 to calculate the efficiency. The brushless-dc drive was a 120 V single-phase unit. It was driving a 1 hp 3-phase motor. The full load was applied to the motor at 1100 rpm and the 50% load at 800 rpm. The input power to the motor was measured in the 3-phase 3-wire configuration which requires two wattmeters. The PWM induction drive was a 230 V 3-phase device. It was loaded by a 5 hp 3-phase induction motor. The speed of the motor was set to 1712 rpm at full load and 1301 rpm at 50% load. The input power to the drive was measured by the reference meter. The input power to the motor was measured in the 3-phase 3-wire configuration.

The results of the drive efficiency measurements are summarized in Table 3.3. It can be seen that the highest percentage errors were obtained for the switched-reluctance technology. It can be attributed to a high harmonic content of the voltage waveform and a low level of measured currents. Meter_2 turned out to be the most

Table 3.3: Converter Efficiencies at Full and 50% Load as Determined by Different Power Meters

ASD Type	Load	R	M1	%E1	M2	%E2	M3	%E3
Switched-Reluctance	Full	92.69	95.56	3.10	95.35	2.87	95.88	3.44
	50%	91.18	94.03	3.13	93.91	2.99	93.85	2.93
Brushless-dc	Full	91.53	96.79	5.75	91.42	-0.12	91.60	0.08
	50%	90.28	90.94	0.73	90.25	-0.03	90.05	-0.25
PWM Induction	Full	95.38	99.86	4.70	96.62	1.30	97.23	1.94
	50%	95.99	92.17	-3.98	96.36	0.39	96.90	0.95

Legend:
R – reference meter
M1 – Meter_1
M2 – Meter_2
M3 – Meter_3
%E1 – percentage error of Meter_1
%E2 – percentage error of Meter_2
%E3 – percentage error of Meter_3

accurate, followed closely by Meter_3. The high percentage errors of Meter_1 indicate that it is not suitable for ASD's applications.

3.2.2 Computer-Controlled Environment

A big advantage of using a computer-controlled environment in testing is the repeatability of applied waveforms and, therefore, the possibility of achieving highly accurate testing results. Two synchronized arbitrary waveform generators (AWG's) were used for this experiment. One of them was driving a voltage amplifier. The other was driving a transconductance amplifier. One period of current and voltage waveforms captured during tests with ASD's and motors was downloaded from a PC to AWG's. A phantom loading method was used to test the meters. The output of the voltage amplifier was applied to the parallel connected voltage terminals of all three channels of the meter under test. The current output of the transconductance amplifier was applied to the series connected current terminals of the tested meter.

The rms values of the applied voltage and current waveforms was measured using the ac measurement standard and the precision current shunt described in Section 3.1. This means that the reference meter was calibrated for *every* measurement.

The nonsinusoidal voltage and current waveforms used during the test are depicted in Figs. 2.2-2.6 and described in Section 2.1. The rms values of the current applied to the meters is given in the tables of results. The rms values of the voltage was 125 V for the sinusoidal tests, 135 V for the PWM inverter input, 165 V for the PWM inverter output, and 130 V for the single-phase rectifier input. The high-frequency components of the input voltages to the brushless-dc motor and to the switched-reluctance motor were beyond the bandwidth of the voltage amplifier. For those two tests, the output of the AWG was connected to the meters through another low-gain wide-bandwidth amplifier. The rms values of the applied voltages were 11 V for the brushless-dc motor case and 17 V for the switched-reluctance motor waveform.

The test results for Meter_1 are given in Table 3.4. It can be seen that high errors of the order of 1% exist for current measurements. Consequently, the power measurements exhibits errors of the same order for sinusoidal tests. Therefore, the power measurement results of Meter_1 for the distorted waveforms are also not reliable. The relatively old model of Meter_1 proved itself to be not suitable for ASD's applications.

Table 3.5 gives test results for Meter_2. The measurements of this meter were the most accurate among the three tested units. The accuracy of rms voltage measurements was within specified limits for all cases. Higher than specified rms current measurement errors were for the case of the brushless-dc and switched-reluctance motors. The power measurement accuracy was adversely affected by decreasing power factor in the sinusoidal test. Unacceptable power measurement errors occurred for the brushless-dc and switched-reluctance motors waveforms.

Table 3.4: Test Results for Meter_1

Waveform type		Percentage Errors of Meter_1 Readings								
		V_A	V_B	V_C	I_A	I_B	I_C	P_A	P_B	P_C
Sinusoidal test	I = 15 A	0.054	-0.026	0.110	1.083	0.651	0.268	1.209	0.621	0.374
PF = 1	I = 7.5 A	0.087	0.006	0.143	0.787	0.325	0.149	0.894	0.328	0.306
Sinusoidal test	I = 15 A	0.100	-0.004	0.148	0.688	-0.388	-0.266	0.338	-0.665	-0.546
PF = 0.5	I = 7.5 A	0.084	-0.028	0.132	1.283	0.417	0.430	1.253	0.410	0.527
PWM inverter	I = 11 A	-0.011	-0.115	-0.004	0.997	0.457	0.192	1.148	0.440	0.215
input	I = 5.5 A	-0.006	-0.102	0.016	1.022	0.370	0.158	0.808	0.296	0.105
PWM inverter	I = 18 A	-0.007	-0.177	-0.068	0.996	0.370	0.027	1.025	0.105	0.018
output	I = 9 A	-0.027	-0.196	-0.087	0.896	0.421	0.123	0.942	0.044	-0.009
1-phase rectifier	I = 8 A	0.022	-0.187	0.029	0.915	0.583	0.305	1.540	0.785	0.805
input	I = 4 A	0.108	0.023	0.146	1.036	0.271	0.140	1.179	0.511	0.039
Brushless-dc	I = 4 A	-0.069	-0.185	-0.096	1.080	0.442	0.416	-0.973	-2.182	-1.673
motor	I = 2 A	-0.065	-0.136	-0.038	0.944	0.367	0.250	-0.459	-1.214	-0.856
Switched-reluctance	I = 4 A	-0.101	-0.521	-0.278	1.615	1.962	0.969	5.308	3.969	5.049
motor	I = 2 A	-0.157	-0.382	-0.181	2.111	3.452	2.061	4.771	4.453	4.943

Table 3.5: Test Results for Meter_2

Waveform type		Percentage Errors of Meter_2 Readings								
		V_A	V_B	V_C	I_A	I_B	I_C	P_A	P_B	P_C
Sinusoidal test	I = 15 A	0.010	0.002	0.010	-0.051	-0.051	-0.044	-0.048	-0.059	-0.048
PF = 1	I = 7.5 A	-0.008	-0.024	-0.016	-0.073	-0.060	-0.060	-0.138	-0.149	-0.138
Sinusoidal test	I = 15 A	0.010	-0.006	0.002	-0.086	-0.086	-0.079	-0.946	-0.958	-0.946
PF = 0.5	I = 7.5 A	0.001	-0.015	-0.007	-0.185	-0.185	-0.185	-1.954	-1.976	-1.954
PWM inverter	I = 11 A	0.013	-0.001	0.006	-0.128	-0.128	-0.119	0.235	0.224	0.235
input	I = 5.5 A	0.004	-0.019	-0.011	-0.264	-0.264	-0.264	0.075	0.053	0.075
PWM inverter	I = 18 A	0	-0.012	-0.006	-0.083	-0.083	-0.071	-0.099	-0.099	-0.099
output	I = 9 A	-0.012	-0.024	-0.018	-0.129	-0.118	-0.129	-0.090	-0.179	-0.090
1-phase rectifier	I = 8 A	-0.007	-0.022	-0.015	-0.061	-0.061	-0.061	0.589	0.589	0.589
input	I = 4 A	0.009	-0.014	-0.006	-0.149	-0.149	-0.149	0.502	0.502	0.502
Brushless-dc	I = 4 A	-0.059	-0.065	-0.059	-1.464	-1.488	-1.488	2.940	2.940	2.940
motor	I = 2 A	-0.047	-0.053	-0.030	-0.493	-0.484	-0.498	6.112	6.129	6.121
Switched-reluctance	I = 4 A	-0.039	-0.048	-0.030	-0.139	-0.139	-0.139	-2.287	-2.287	-2.287
motor	I = 2 A	-0.041	-0.059	-0.059	-0.498	-0.503	-0.478	-1.830	-1.830	-1.743

The test results for Meter_3 are summarized in Table 3.6. The meter performed well for rms voltage measurements. However, current and power measurements are in most cases much higher than specified in the manual.

3.2.3 Additional Tests

Additional test were conducted for the best performing Meter_2. The influence of frequency at unity power factor and the power factor at the fundamental power grid frequency was investigated. The accuracy of the meter for different frequencies at V_{rms} = 125 V, I_{rms} = 15 A, and unity power factor is presented in Table 3.7. The meter readings were within the accuracy range specified by the manufacturer.

The percentage errors of Meter_2 for different power factors at 60 Hz sinusoidal waveforms with V_{rms} = 125 V and I_{rms} = 15 A are given in Table 3.8. It can be seen that the power measurement errors are higher than specified starting from power factor $PF = 0.74$.

3.3 Meter Evaluation Criteria

The ASHRAE sponsoring committees supplied the Florida Power Quality and Power Electronics Laboratory (PQ&PE Lab) with a list of criteria [22] that need to be considered during evaluation of the tested meters. The criteria in order of importance are: accuracy and repeatability, quality and reliability, technical support (how the instrument is designed and Internal Code), field use versus laboratory use, ease of use, repair and calibration services, cost, technical support contract, and warranty. A questionnaire on the criteria was prepared and sent to the manufacturers. Responses to the questionnaire were received from Meter_2 and Meter_3 manufacturers' representatives. The manufacturer of Meter_1 did not cooperate with the PQ&PE Lab in this project and it did not return an answered questionnaire. The following

Table 3.6: Test Results for Meter_3

Waveform type		Percentage Errors of Meter_3 Readings								
		V_A	V_B	V_C	I_A	I_B	I_C	P_A	P_B	P_C
Sinusoidal test	I = 15 A	-0.020	-0.020	-0.036	-0.083	-0.034	-0.055	-0.134	-0.077	-0.113
PF = 1	I = 7.5 A	-0.017	-0.017	-0.033	-0.209	-0.167	-0.181	-0.260	-0.204	-0.239
Sinusoidal test	I = 15 A	-0.016	-0.008	-0.024	-0.098	-0.056	-0.077	-3.409	-3.338	-3.375
PF = 0.5	I = 7.5 A	-0.022	-0.022	-0.038	-0.207	-0.151	-0.165	-3.412	-3.360	-3.414
PWM inverter	I = 11 A	-0.010	-0.003	-0.025	-0.314	-0.270	-0.296	5.280	5.337	5.291
input	I = 5.5 A	-0.023	-0.015	-0.037	-0.194	-0.158	-0.176	5.338	5.395	5.354
PWM inverter	I = 18 A	-0.014	-0.002	-0.032	-0.191	-0.139	-0.162	-4.186	-4.130	-4.178
output	I = 9 A	-0.017	-0.005	-0.035	-0.128	-0.083	-0.094	-4.044	-3.988	-4.035
1-phase rectifier	I = 8 A	-0.024	-0.008	-0.039	-0.398	-0.358	-0.385	1.360	1.422	1.381
input	I = 4 A	0.029	-0.022	-0.045	-0.964	-0.937	-0.937	0.794	0.851	0.807
Brushless-dc	I = 4 A	-0.046	-0.046	-0.073	-0.739	-0.696	-0.974	-5.943	-5.900	-6.187
motor	I = 2 A	-0.012	-0.012	-0.039	-2.555	-2.509	-2.786	-6.691	-6.643	-6.931
Switched-reluctance	I = 4 A	-0.007	-0.013	-0.037	-0.905	-0.787	-1.046	6.492	6.529	6.152
motor	I = 2 A	-0.053	-0.059	-0.083	-3.084	-2.982	-3.222	3.573	3.621	3.255

Table 3.7: Test Results for Meter_2 at $V_{rms} = 125$ V, $I_{rms} = 15$ A, and $PF = 1$.

Sinusoidal Test Frequencies (Hz)	Percentage Errors of Meter_2 Readings								
	V_A	V_B	V_C	I_A	I_B	I_C	P_A	P_B	P_C
60	0.010	0.002	0.010	-0.051	-0.051	-0.044	-0.048	-0.059	-0.048
600	-0.006	-0.022	-0.014	-0.056	-0.056	-0.050	-0.064	-0.080	-0.064
1200	0.006	-0.010	-0.002	-0.038	-0.044	-0.031	-0.043	-0.059	-0.043
1800	-0.004	-0.020	-0.020	0.076	0.076	0.090	0.070	0.054	0.075
2400	0.006	-0.011	-0.002	-0.020	-0.020	-0.007	-0.016	-0.033	-0.011
3000	0.007	-0.010	-0.002	0.227	0.241	0.227	0.230	0.219	0.236

Table 3.8: Test Results for Meter_2 at $V_{rms} = 125$ V and $I_{rms} = 15$ A.

Sinusoidal Test at 60 Hz	Percentage Errors of Meter_2 Readings								
	V_A	V_B	V_C	I_A	I_B	I_C	P_A	P_B	P_C
$PF = 1$	0.010	0.002	0.010	-0.051	-0.051	-0.044	-0.048	-0.059	-0.048
$PF = 0.93$	-0.005	-0.021	-0.013	-0.066	-0.066	-0.060	-0.149	-0.161	-0.149
$PF = 0.74$	0.010	-0.006	0.002	-0.066	-0.066	-0.060	-0.331	-0.345	-0.331
$PF = 0.46$	-0.002	-0.010	-0.002	-0.080	-0.080	-0.073	-0.709	-0.720	-0.709
$PF = 0.13$	0.006	-0.010	-0.002	-0.076	-0.069	-0.069	-2.16	-2.20	-2.16

review of the tested meters features according to the criteria is based on the author's experiences and manufacturers' responses.

Accuracy and Repeatability

This the most important criterion in determining meters usefulness in adjustable speed drive applications. The accuracy of the meters was tested under various conditions as described in the preceding sections. The test results presented in Tables 3.3 through 3.6 show that Meter_2 is the most accurate meter. It must be noted that even Meter_2 exhibited unacceptably high power measurement errors for the brushless-dc and switched-reluctance motors waveforms.

Quality and Reliability

The meters were tested in a laboratory environment. Neither of the meters caused any technical problems during operation. The Meter_3 series carries full ISO9001 certification.

Technical Support

Technical support is available for all the meters through manufacturers representatives. The modular design of Meter_3 allows for a customized configuration of up to 6-phase measurements. Additional modules need to be purchase to take advantage of this possibility. The other two meters are limited to 3 input modules.

Field Use versus Laboratory Use

All the meters were designed primarily for use in controlled environments. However, their size and mechanical design allows with a careful handling for a limited field use wherever 120 V ac power supply is available. Built-in printers are useful features for Meter_2 and Meter_3 for both laboratory and possible field use.

Ease of Use

Meter_2 was found to be the most user friendly instrument among tested meters. It was due to the fact that all the settings of Meter_2 are accessible via a separate function key including a LED to indicate the setting. Large LED display of Meter_2 is able to display four measured parameters simultaneously. However, Meter_3 is equipped in the most flexible and sophisticated display, that is, graphics compatible electroluminescent monitor. It can display 3, 12, or 36 freely selectable measured values, harmonic spectral analysis in table or bar-chart form, parameters of individual harmonics, on-line help, measured values in table form, and stored waveforms. The drawbacks of Meter_3 are that it requires a manual change of current shunts when the range of current measurement is to be changed and that it is menu driven which makes it sometimes tedious to change a selected parameter of a measurement. Both Meter_2 and Meter_3 come with well-written and easy-to-follow manuals. As was already mentioned, both those meters have internal printers installed that increases user friendliness. Meter_1 was found to be not user friendly. Small LED display for 4 parameters, partially menu-driven change of settings, typewritten manual with very few illustrations and without an index or a good table of contents, as well as lack of internal printer make it difficult to operate.

Repair and Calibration Services

Repair services are available through manufacturers representatives. The manufacturer of Meter_2 has a fully NIST traceable calibration laboratory in Georgia. Modular design of Meter_3 allows for field replacement of modules to be repair or calibrated without requiring subsequent calibration.

Cost

The cost of a fully loaded 3-phase Meter_2 was $16,195 at the day of the loan. The price of a comparable Meter_3 configuration was about $23,000. Meter_1

is no longer available for purchase because new models have been introduced by the manufacturer.

Technical Support Contract

Technical support contract is presently not available for any of the meters.

Warranty

Meter_3 is warranted for 2 years limited to 1 year on calibration. Meter_1 and Meter_2 come with a 1 year warranty.

3.4 Metering Implications of Waveforms Harmonic Content

The rms values of voltage and current are calculated by modern power meters and analyzers as

$$V = \sqrt{\frac{1}{N}\sum_{k=1}^{N} v^2(k)} \text{ and } I = \sqrt{\frac{1}{N}\sum_{k=1}^{N} i^2(k)}. \tag{3.2}$$

The real power is obtained as an average value of the instantaneous power $p(t) = v(t)i(t)$

$$P = \frac{1}{N}\sum_{k=1}^{N} v(k)i(k). \tag{3.3}$$

The apparent power is calculated from voltage and current rms values

$$S = VI. \tag{3.4}$$

The meters calculate the reactive power according to Fryze's definition [13] as

$$Q = \sqrt{S^2 - P^2}. \tag{3.5}$$

The voltage, current, power, and efficiency measurement accuracy of three digital power meters and analyzers were laboratory tested. The results are presented in Section 3.2. Waveforms of Figs. 2.2–2.6 were applied to the meters during tests.

Technical specifications of the tested meters are presented in Section 3.1. Let us recall the meters' parameters related to bandwidth and harmonic analysis. The bandwidth of Meter_1 is dc and 0.1 Hz–200 kHz. Harmonic analysis is performed up to 50 components using discrete Fourier algorithm. The maximum sampling frequency for the 3-phase configuration is 95 kHz. The measurement bandwidth of Meter_2 is dc and 2 Hz–200 kHz. 50 harmonic components are calculated using 8192 points FFT. The maximum sampling frequency is 104 kHz. Meter_3 has the measurement bandwidth dc–400 kHz. Up to 99 harmonics are calculated using Discrete Fourier Transform. The maximum sampling frequency is 70 kHz.

A higher measurement bandwidth than the sampling frequency is achieved by the meters with an equivalent waveform method. It is assumed that the measured waveform is periodic. A period of an equivalent waveform is created from samples collected over several periods of the measured waveform. The periodicity assumption does not, however, hold for the real-world ASD waveforms which in a *quasi* steady-state. That is, the measured values of the voltage, current, and power oscillate around equilibrium points. For instance, it was measured that those oscillations can amount to 6% of the equilibrium value during a time span of twenty periods for the current waveform in the switched-reluctance motor.

The second meter was able to measure with a satisfactory accuracy input powers to the drives and the input power to the induction motor. All meters failed to measure accurately powers and the input to the brushless-dc and to the switched-reluctance motor. The active power measurement errors were up to 7%. This inaccuracy can be attributed to a high content of high-frequency harmonics in voltage spectra and, consequently, in instantaneous power spectra. With a sampling frequency only about 5 times higher than substantial harmonics in the instantaneous power waveform, the meters were unable to accurately recreate the power waveform for further processing. For practical purposes, the sampling frequency should be

at least 10 times higher than the most significant harmonic. Thus, an increase in sampling frequency to a few hundreds of kilohertz is needed to improve accuracy of power measurements in ASD's applications. The equivalent waveform method should be abandoned. More advanced synchronization circuits should also be used that allow for synchronization to highly distorted waveforms and independent synchronization of different channels.

Harmonic analysis up to the first 50 or even 100 components is not enough for ASD applications (see Figs. 2.3, 2.5, and 2.6). Taking into account the 50 most significant harmonics does not also accurately reflect frequency spectra of the voltage waveforms of inverter-fed PWM induction, brushless-dc, and switched-reluctance motors (see Figs. 2.7–2.9 and Table 2.2). With an increase in the sampling frequency, modern power meters should provide harmonic analysis with several hundreds of components. There should be a tool to group and order harmonics according to their frequency and magnitude.

The precision power meter and analyzer manufacturers are becoming aware of challenges in power measurements that are posed by proliferation of power electronic devices, especially by ASD's and electronic ballasts. Meters that fulfill the abovementioned requirements are planned to be marketed in a very near future. Laboratory tests will be needed to determine if the new models meet users' expectations of power measurement accuracy under highly nonsinusoidal conditions of a few tens of a percent [23].

CHAPTER 4
TESTING PROCEDURES FOR ASD'S AND MOTORS

4.1 Equipment

4.1.1 Instrumentation

Over 15 transducer manufacturers were contacted to request written literature on their transducers. Twelve of these manufacturers responded and sent company literature which was reviewed, compiled, and analyzed for voltage and current transducers. Table 4.1 shows the list of these manufacturers, the rated accuracy of their "best" voltage and current transducers, the frequency range for such transducers, and some comments about them.

None of the voltage transducers described in Table 4.1 is designed to measure voltages greater than 600 V. Some of the current transducers can measure currents of the order of several hundred amps. However, as can be seen from the table, the accuracy of both voltage and current transducers that can be used together with inexpensive voltmeters is too low for applications in precision power measurements and the bandwidth of those transducers is limited. In the authors opinion, the most accurate presently available method of measuring power for high-voltage and high-power motors and ASD's is to use wide-band potential and current transformers together with laboratory voltage and current probes connected to modern digital power meters. The effects of such transformers on measurement accuracy should be further investigated.

It is important to note that most, if not all, of the manufacturers' literature specify the accuracy of specific products as a single number, which is usually obtained

Table 4.1: Voltage and Current Transducer Manufacturers. Literature-Review Summary.

	Manufacturer	Rated Accuracy	Frequency Range (Hz)	Comments
1	A	±0.25% FS	47-1000	Sensors designed primarily for use with motor protection, automated machinery, process controls, energy management, and load distribution data acquisition applications.
2	B	±0.5%	up to 3rd harmonic	Transducers (for use in electric power distribution) designed for use on waveforms with up to 30% of 3rd harmonic content. Users of these transducers are primarily utilities, and manufacturers of energy management schemes, among others.
3	C	±0.5% FS	3-1000	Sensors that monitor 3-phase power with Hall Effect devices. Primarily used to monitor motor loads.
4	D	±0.25% FS	1-100k	Manufacturer of Hall Effect current sensors. Literature provides, in addition to numbers, many specification plots for different sensors.
5	E	I:±0.4% FS V:±0.25% FS	I: to 100k V: 0-10k	Hall Effect current sensors designed for a.c. pulse and variable frequency drives, and other non-sinusoidal signals.
6	F	n/s	0-25M	Scope voltage probes.
7	G	±0.2%	up to 9th harmonic	Designed to measure ac current signals in single and three-phase systems.
8	H	±0.5%	60	Basic loop powered sensors.
9	I	±0.25% FS	n/s	Some models designed for input to meters, RTUs, SCADA and other substation devices.
10	J	±0.15% FS	up to 9th harmonic	Designed for SCADA devices and substation monitoring.
11	K	±0.2% FS	50-400	Average sensing devices calibrated for RMS value of sine wave.
12	L	n/s	?-12M	Very vague literature. Some of their devices produce some distortion, but no quantification about it is given.

NOTES: n/s = not specified in literature. FS = full scale
MANUFACTURERS:
A – American Aerospace Controls Inc.
B – Crompton Instruments Inc.
C – Load Controls Inc.
D – Jenesco Inc.
E – Ohio Semitronics Inc.
F – PMK (German company) distributed by Oregon Analog Tools Inc.
G – PC&S multitek
H – Riley Corporation Sales Inc.
I – Rochester Instrument Systems Inc.
J – Scientific Columbus
K – TransData Inc.
L – T&M Research Products Inc.

under pure (i.e., 0% THD) sinusoidal conditions, at a specific frequency, and at a specific voltage or current. However, the accuracy of a probe is most useful when specified as a plot of frequency response, which would include at least two plots: %Error for magnitude versus frequency, and %Error for phase shift versus frequency.

Furthermore, and better yet, accuracy should be specified as plot which consists of a family of curves at different magnitude levels and for different frequencies. Ideally, accuracy of a device should be specified as a "surface" rather than as a number. For example, most probably, the frequency response of a voltage transducer at a frequency range of, say, 45 to 3000 Hz, at a voltage of 0.1 Volts is different than the frequency response of the same transducer at a voltage of 120 V, and of course, for some other magnitudes in between (see Fig. 4.1).

As could be seen in Table 4.1, the transducers currently available on the market for low-cost high-voltage and high-current application have an accuracy of the order of a few tens of percent and a limited bandwidth. In order to accurately measure input power to induction motors, the bandwidth of transducers should be at least 3000 Hz as specified by IEEE Std 119. The harmonic content of power waveforms for brushless-dc and switched-reluctance motors is higher (see Figs. 2.5 and 2.6) with substantial harmonics of the 200th order present. Thus, transducers for applications to these motors should have a bandwidth of around 20 kHz. When those criteria were presented to the manufacturers in phone conversations, the response was that they do not expect to introduce such transducers to the market in the near future. The currently available transducers are used mainly in panel and control instrumentation. Further, it is not cost-efficient to try to develop a new family of accurate wide-bandwidth transducers when no big market demand for them is anticipated.

The testing results of modern solid-state power meters and analyzers presented in Chapter 3 also show that these meters do not measure accurately power at the input to brushless-dc and switched-reluctance motors. However, in this case, since

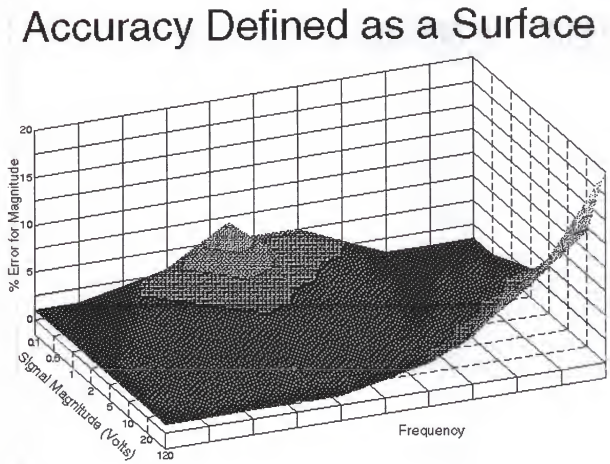

Figure 4.1: An example of a suggested accuracy surface (figure reprinted with a permission from [24]).

the meters are intended for use under highly distorted voltage and current conditions, the manufacturers show a great interest in ideas for the improvement of their products performance. The authors suggestions for improving accuracy is to increase 3-4 times the sampling frequency of the meters which for the tested units was of the order of 100 kHz. Additionally, the synchronization circuits should be modified to allow for synchronization to highly distorted waveforms and independent synchronization of different channels.

Recently, a power meter was introduced to the market whose parameters listed in the manual would make it suitable for power measurements of inputs to brushless-dc and switched-reluctance motors. The meter has a sampling frequency of 500 kHz, calculates up to 2047 harmonics, and its channels can be independently synchronized. The basic accuracy of the meter is given as 0.05% in the frequency range of 0.001 Hz – 10 kHz for voltage and current. A demo unit of this meter was obtained for a week-long loan in September, 1995. Accuracy tests in a computer-controlled environment were conducted. It turned out, however, that the unit on loan had a software bug and, consequently, did not correctly processed waveforms with multiple zero crossings. Thus, the accuracy claimed by the manufacturer for the new power meter could not be verified.

4.1.2 ASD's and Motors

There are three main motor technologies used in fractional and integral horse-power adjustable speed air conditioners and heat pumps, namely, induction, brushless-dc, and switched-reluctance motors. The choice of a particular type of motor and consequently a drive depends on many criteria, e.g., power requirements, initial cost, life-cycle cost, efficiency, dynamic performance, ease of maintenance, power density, reliability, and environmental requirements.

Induction motors are the most widespread non-commutator motors. They are powered by a three-phase alternating voltage or current source. Fig. 4.2(a) shows schematically a cross section of a two-pole induction motor. Three-phase windings are placed in slots in the stator. The windings are located so that their current generates an approximately sinusoidally distributed flux density around the perimeter of the air gap. Squirrel-cage rotors have aluminum bars cast into slots in their outer periphery. These bars are shorted at both ends of the rotor. Induction motors require little maintenance. They are reliable and efficient in medium and high-power applications. In low power and low speed applications, however, they may have problems with overheating.

Brushless-dc motors are also known as switched or trapezoidal permanent magnet (PM) motors. A cross section of a brushless-dc motor is shown in Fig. 4.2(b). The physical structure of the stator is similar to that of an induction motor but the windings of each phase are distributed over two arcs of 60°. Nearly rectangular current pulses are supplied sequentially to each of the three stator phases to produce the electromagnetic force that atracts the permanent magnet of the rotor. In a two-pole design, six-steps of the switching action result in one rotor revolution. Rotor position sensors, e.g., hall-effect transducers, are required for proper timing of current pulses. Theoretically, PM motors should be more efficient than induction motors because they have no equivalent of the energy loss in the rotor bars as do induction motor. The initial cost of a brushless-dc motor is high due to the complicated manufacturing process. PM motors have an excellent dynamic response.

A cross section of a switched-reluctance motor is depicted in Fig. 4.2(c). The motor has a doubly salient structure. The most popular are 6/4 (3-phase, 6 stator poles, 4 rotor poles), 8/6 (4-phase), and 10/8 (5-phase) motors. Each stator pole is surrounded by a coil. Connected in series, opposite stator poles form a one phase winding. The manufacturing costs of switched reluctance motors are low. The

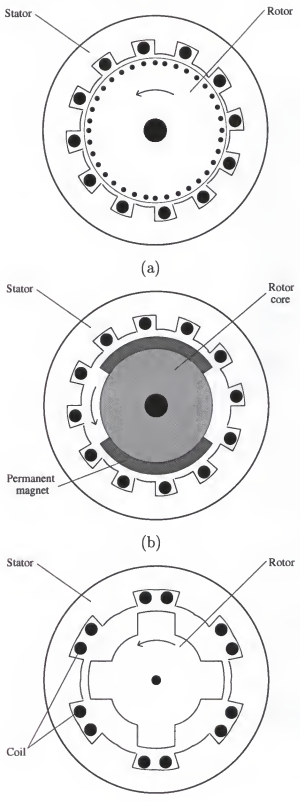

Figure 4.2: Schematic cross sections of motors. (a) Induction motor. (b) Brushless-dc motor. (c) Switched-reluctance motor.

efficiency of switched-reluctance motors is comparable to that of induction motors of similar power ratings. Switched-reluctance motors require little maintenance and have a good dynamic response. They may have a high torque ripple due to the doubly salient structure. The design of a switched-reluctance motor is very closely related to the design of its power converter and a controller that are parts of a switched-reluctance drive.

PWM inverters for adjustable speed drive applications are shown in Fig. 4.3. The inverters have insulated-gate bipolar transistors (IGBT's) as active switches. A three-phase PWM inverter that is suitable for use with induction and brushless-dc motors is shown in Fig. 4.3(a). Motor windings are connected to the terminal between IGBT's in each switching leg. Fig. 4.3(b) shows a three-phase PWM inverter for a switched reluctance motor. It can be seen that the motor windings are inherent parts of the inverter. In such a structure, it is usually difficult to access the motor terminals. Thus, a switched reluctance motor and drive should be specially prepared by qualified personnel for laboratory testing that involves measurements of motor electrical quantities.

4.2 Measurement Procedures

The present industry standards [25]-[27] give testing methods that can be followed to obtain the energy efficiency of induction, synchronous, and dc motors; however, these standards specify that the energy efficiency tests on motors are to be conducted under pure sinusoidal or constant dc input voltage. This is not the case when ASDs are used. Thus, these established industry standards cannot be followed step by step to obtain the energy efficiency of motor-ASD sets under nonsinusoidal power conditions.

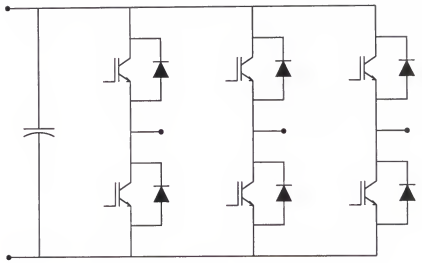

(a)

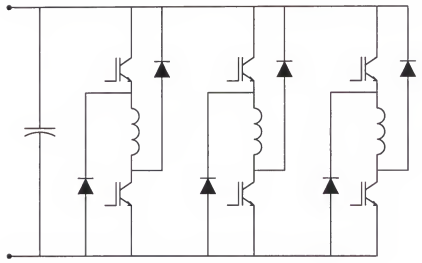

(b)

Figure 4.3: PWM inverters. (a) For induction and brushless-dc motors. (b) For switched-reluctance motor.

For the case of induction motors, the most commonly used standards to test their energy efficiency is IEEE Std 112-1984 which is used to perform tests on polyphase induction motors and generators. This standard gives the test method which is used in the National Energy Efficiency Act approved by the House and the Senate of the United States and signed into law in 1992. When testing induction motors, this standard should be followed where possible.

Other industry standards can be followed to perform energy efficiency tests on induction motors. These standards, CSA 390-1985, IEEE Std 114-1982, ANSI C50.20, and others, give detailed test procedures. These procedures are based on the one outlined in IEEE Std 112-1984.

The preferred method of measuring mechanical output power of fractional and integral motors is by loading the machine with a dynamometer where the dynamometer is defined as a load absorber equipped with means for indicating torque and speed [25]. To obtain accurate readings the dynamometer rating shall not exceed three times the machine rating and the dynamometer sensitivity shall be 0.25% of the machine rated torque.

Three main parameters determine the operating point of an ASD-motor set with a stable power supply and constant ambient temperature, namely, the machine rotating speed, the machine load, and the machine windings temperature. The machine desired speed and load testing points should be determined prior to the experiment based on manufacturer's data and testing facility needs. Examples of such speed/load testpoint sets are: constant-speed/variable load, variable-speed/constant load, or a speed/load curve of a certain device (for instance, a fan). The testpoint sets should contain at least several speed/load combinations so that graphical presentation of data is possible. The measurement of the machine windings temperature should be done using thermocouples or resistance temperature detectors (RTD's) as outlined in [25] p. 21. General information on temperature measurements as applied

Table 4.2: Nameplate Data of the Induction Motor Under Test.

POWER RATING		TYPE	
# OF PHASES		BRAND	
VOLTAGE		DESIGN	
FULL LOAD AMPS		FRAME	
FREQUENCY		DUTY	
RATED SPEED		INS. CLASS	

to electrical apparatus is provided in [28]. The correction of a measured winding resistance to any temperature can be done using

$$R_s = R_t \frac{t_s + k}{t_t + k} \ (\Omega) \tag{4.1}$$

where R_s (Ω) is the winding resistance corrected to specified temperature t_s (°C), R_t (Ω) is the test value of winding resistance, t_s (°C) is the temperature of winding when the resistance was measured, and constant k is 234.5 for pure copper and 225 for aluminum based on a volume conductivity of 62% (suitable value of k must be used for other winding materials). The winding losses can be determined from

$$P_{WL} = nR_sI^2 \ (\mathrm{W}) \tag{4.2}$$

where n is the number of phases and I is the rms value of the motor phase current.

4.2.1 Squirrel Cage Induction Motor-ASD Set Testing Procedure

The following testing procedure should be followed to obtain the efficiency of an integral hp induction motor-ASD set at different load/speed combinations. The name plate data and specifications of the motor should be tabulated as in Table 4.2.

Induction motor testing procedure without ASD

The following procedure should be followed to obtain an integral hp induction motor (IM) equivalent circuit in order to calculate its copper losses during the drive test. The no-load test results give the core, friction, and windage losses.

1. Perform the no-load test on the IM as specified in [25] pp. 14-15.

2. Perform the locked-rotor test on the IM as specified in [25] pp. 15-17.

3. From the no-load and locked-rotor test results, calculate the IM equivalent circuit parameters using the procedure from [25] p. 30.

   The following program was written to calculate the IM equivalent circuit parameters by iteratively solving a set of three equations from [25] p. 30. As an example, input data obtained for a 3-phase NEMA B design energy-efficient 5 hp induction motor are used.

```
% Program for solving the IEEE-112 p.30 system of equations
%
% VL - phase voltage, volts
VL=31.293;
% IL - line current, amperes
IL=13.72;
% WL - power, watts
WL=311.5;
% VO - no-load test phase voltage, volts
VO=131.7;
% IO - no-load line current, amperes
IO=4.653;
% WO - no-load test power, watts
WO=131.7;
% m - number of phases
m=3;
% ffL - ratio of rated frequency to impedance-test frequency
ffL=1;
% x1x2 - ratio of stator leakage reactance to rotor leakage
%        reactance referred to stator; when design details are
%        not available, use 1.0 for Design A motors, 0.67 for
%        Design B, and 0.43 for Design C
x1x2=0.67;
% r1p - stator resistance at temperature during no load
%       test, ohms
r1p=0.45;
% r1dp - stator resistance at temperature during impedance
%        test, ohms
r1dp=0.45;
% Wf - friction and windage loss, watts
Wf=38;
% x1 - stator leakage reactance, ohms
x1=10.851;
% xM - magnetizing reactance, ohms
xM=517;
x1xM=x1/xM;
```

```
VARL=sqrt((m*IL*VL)^2+WL^2);
VARO=sqrt((m*IO*VO)^2+WO^2);

for i=1:100,
    xMo=xM;
    xM=(m*VO^2/(VARO-m*IO^2*x1))*(1/(1+x1xM))^2;
    x1L=(VARL/(m*IL^2*(1+x1x2+x1xM)))*(x1x2+x1xM);
    x1o=x1;
    x1=ffL*x1L;
    x1xM=x1/xM;
    if ((abs(x1-x1o)/x1)<0.001 & (abs(xM-xMo)/xM)<0.001),
      break;
    end;
end;

% bM - magnetizing susceptance, 1/ohms
bM=1/xM;
% x2 - rotor leakage reactance referred to stator, ohms
x2=x1/x1x2;
% Wh - core loss, watts
Wh=WO-Wf-m*IO^2*r1p;
% gfe - core conductance, 1/ohms
gfe=(Wh/(m*VO^2))*(1+x1xM)^2;
% rfe - core resistance, ohms
rfe=1/gfe;
% r2dp - rotor resistance referred to stator at temperature
%        during impedance test, ohms
r2dp=((WL/(m*IL^2))-r1dp)*(1+x2/xM)^2-(x2/x1)^2*(x1L^2*gfe);
```

The calculated in 5 iterations motor parameters are $bM = 0.0367$, $x2 = 1.4489$, $Wh = 64.4719$, $gfe = 0.0013$, $rfe = 752.5302$, and $r2dp = 0.1099$.

Squirrel cage induction motor-ASD set testing procedure

1. Couple the motor to the dynamometer by means of a flexible coupling and align the shaft of the motor to the shaft of the dynamometer.

2. Electrically, connect the motor to the ASD according to their manufacturer(s) manuals, and install a temperature measuring devices (thermocouples or RTD's) in the motor stator windings.

3. Connect a three-phase power meter at the input of the motor using the three voltages and three currents configuration and another three-phase power meter

at the input of the ASD using the same connection configuration. This connection allows for monitoring phase currents and line voltages. If only the power is to be measured, the 3-phase/3-wire connection can be used.

4. Apply rated voltage to the input of the IM ASD.

5. Using the ASD, set the speed of the motor to the speed at which the test needs to be conducted.

6. Using the dynamometer controller, set the torque of the motor to the value at which the test needs to be conducted.

7. Monitor the temperature reading until it becomes stable. The temperature can be assumed to be stable when the reading does not change by more than 0.5°C over a 1 minute period time.

8. Record values of power, current, and temperature in Tables 4.3 and 4.4.

9. Repeat steps 5-8 for other speed/load combinations of the testpoint set.

10. Calculate losses and efficiencies of the motor, ASD, and motor-ASD set at steady-state efficiency points according to Table 4.3.

11. Plot losses and efficiency curves for the motor, ASD, and the variable speed drive system versus speed or load.

12. Perform separation of losses for the motor as outlined in [25] and tabulate the results in Table 4.4.

4.2.2 Brushless dc Motor-ASD Set Testing Procedure

As stated by the manufacturer, the technological constraints of the brushless-dc motor and its controller do not allow for no-load tests during which the motor

Table 4.3: Induction Motor-ASD Separation of Losses and Efficiencies

MOTOR DATA				ASD DATA		LOSSES			EFFICIENCY		
1	2	3	4	5	6	7	8	9	10	11	12
Torque (Nm)	Speed (rpm)	Output Power (W)	Temp. (°C)	Input Power (W)	Output Power (W)	Motor (W)	ASD (W)	System (W)	Motor (%)	ASD (%)	System (%)
.											
.											
.											
.											
.											
.											
.											
.											
.											
.											

Relationships among columns:
$(3) = 2\pi \times (1) \times (2)/60$
$(7) = (6) - (3)$
$(8) = (5) - (6)$
$(9) = (5) - (3) = (7) + (8)$
$(10) = 100 \times (3)/(6)$
$(11) = 100 \times (6)/(5)$
$(12) = 100 \times (3)/(5) = (10) \times (11)/100$

Table 4.4: Induction Motor Separation of Losses

MOTOR DATA						LOSSES					
1	2	3	4	5	6	7	8	9	10	11	12
Input Power (W)	Torque (Nm)	Speed (rpm)	Output Power (W)	Input Current (A)	Stator Temp. (°C)	Motor Total (W)	Fric. & Wind. (W)	Stator (W)	Core (W)	Rotor (W)	Stray Load (W)

Relationships among columns:
$(4) = 2\pi \times (2) \times (3)/60$
$(7) = (1) - (4)$
$(7) = (8) + (9) + (10) + (11) + (12)$

would run at a higher speed than customer dictated upper end speed. Also, the motor should not be run without the ASD because of a possible permanent demagnetization. Testing procedures proposed in this section are designed to obtain the most important performance information, that is, separation of losses between the motor and the power electronic controller. Additionally, copper losses can be calculated using (4.2).

The following procedure should be followed to obtain the losses and efficiencies of a brushless dc motor-drive system under different load/speed combinations:

1. Couple the dc motor to the dynamometer by means of a flexible coupling and align the shaft of the motor to the shaft of the dynamometer.

2. Connect the input and the output of the ASD to the power meter. In case of a 1-phase input/3-phase output ASD, use 1-phase/2-wire connection at the input and 3-phase/3-wire connection at the output of the ASD. Two power meters are needed in case of a 3-phase input ASD.

3. Insert a temperature measuring device into the armature of the motor.

4. Measure the value of the line-to-line armature resistance of the "cold motor" and the ambient temperature.

5. Install external cooling devices for the motor and the ASD as specified by the manufacturer.

6. Apply rated voltage to the input terminal of the variable speed brushless dc drive through a protection circuitry.

7. Using the dynamometer controller, set the speed of the motor to the speed at which the test needs to be conducted.

8. Using the variable speed motor controller, set the motor torque to the value at which the test needs to be conducted.

9. Monitor the temperature reading until it becomes stable. Adjust torque and speed values which may be affected by the temperature change. Do not exceed manufacturer specified temperature ratings. The temperature can be assumed to be stable when the reading does not change by more than 0.5°C over a 1 minute period time.

10. Record values of power, current, and temperature in Table 4.5.

11. Repeat steps 7-10 for other speed/load combinations of the testpoint set.

12. Calculate the losses and efficiencies of the motor, ASD, and the motor-ASD set at each steady-state efficiency point and record the results in Table 4.5.

13. Plot losses and efficiency curves for the motor, ASD, and the variable speed drive system versus speed or load.

4.2.3 Switched-Reluctance Motor-ASD Set Testing Procedure

The principle of operation of a switched-reluctance motor does not allow one to run the motor without a converter. The copper losses in the motor can be determined from (4.2).

The following procedure should be followed to obtain the efficiency of a switched-reluctance motor and its power electronic controller at different load/speed combinations:

1. Couple the switched-reluctance motor to the dynamometer by means of a flexible coupling and align the shaft of the motor to the shaft of the dynamometer.

2. Connect the variable-speed switched-reluctance drive to the power supply through an appropriate protection circuitry.

Table 4.5: Brushless dc Motor-ASD Separation of Losses and Efficiencies

MOTOR DATA				ASD DATA		LOSSES			EFFICIENCY		
1	2	3	4	5	6	7	8	9	10	11	12
Torque	Speed	Output Power	Temp.	Input Power	Output Power	Motor	ASD	System	Motor	ASD	System
(Nm)	(rpm)	(W)	(°C)	(W)	(W)	(W)	(W)	(W)	(%)	(%)	(%)
.											
.											
.											
.											
.											
.											
.											
.											
.											
.											

Relationships among columns:
(3) = $2\pi \times (1) \times (2)/60$
(7) = (6) − (3)
(8) = (5) − (6)
(9) = (5) − (3) = (7) + (8)
(10) = $100 \times (3)/(6)$
(11) = $100 \times (6)/(5)$
(12) = $100 \times (3)/(5) = (10) \times (11)/100$

3. Connect the input and output of the ASD to the terminals of the power meters using an appropriate connection configuration. At least two power meters should be used to record simultaneously the input power to the ASD and the input power to all the phases of the motor. The n-phase/n-wire meter configuration cannot be used for the switched-reluctance motor because motor windings do not have a common terminal.

4. Insert a temperature measuring device into the armature of the motor.

5. Measure the value of the phase armature resistance of the "cold motor" and the ambient temperature.

6. Install external cooling devices for the motor and the ASD as specified by the manufacturer.

7. Apply rated voltage to the input terminal of the variable speed switched-reluctance motor-drive set.

8. Using the variable speed switched reluctance motor controller, set the speed of the SRM to the specified speed at which the test needs to be conducted.

9. Using the dynamometer controller, set the speed of the motor to the speed at which the test needs to be conducted.

10. Monitor the temperature reading until it becomes stable. Adjust torque and speed values which may be affected by the temperature change. Do not exceed manufacturer specified temperature ratings. The temperature can be assumed to be stable when the reading does not change by more than 0.5°C over a 1 minute period time.

11. Record values of power, current, and temperature in Table 4.6.

12. Repeat steps 8-11 for other speed/load combinations of the testpoint set.

13. Plot losses and efficiency curves for the SRM, ASD, and the variable speed motor-drive set.

Table 4.6: Switched-Reluctance Motor-ASD Separation of Losses and Efficiencies

MOTOR DATA				ASD DATA		LOSSES			EFFICIENCY		
1	2	3	4	5	6	7	8	9	10	11	12
Torque (Nm)	Speed (rpm)	Output Power (W)	Temp. (°C)	Input Power (W)	Output Power (W)	Motor (W)	ASD (W)	System (W)	Motor (%)	ASD (%)	System (%)
.											
.											
.											
.											
.											
.											
.											
.											
.											
.											

Relationships among columns:
$(3) = 2\pi \times (1) \times (2)/60$
$(7) = (6) - (3)$
$(8) = (5) - (6)$
$(9) = (5) - (3) = (7) + (8)$
$(10) = 100 \times (3)/(6)$
$(11) = 100 \times (6)/(5)$
$(12) = 100 \times (3)/(5) = (10) \times (11)/100$

CHAPTER 5
WAVELET TRANSFORM ANALYSIS OF ASD WAVEFORMS

5.1 Wavelet Transform versus FFT

The Fourier transform of a continuous time-domain signal $x(t)$ is given by

$$X(f) = \int_{-\infty}^{+\infty} x(t) e^{-j2\pi ft} dt. \tag{5.1}$$

Under certain mathematical assumptions that are practically always fulfilled for real-world electric signals, the Fourier transform is invertible, i.e., the signal can reconstructed in the time domain from the frequency series $X(f)$ using the relationship

$$x(t) = \int_{-\infty}^{+\infty} X(f) e^{j2\pi ft} df \tag{5.2}$$

which is known as the inverse Fourier transform. In digital computer technology, continuous signals are sampled N times per period. To process such sampled data, discrete versions of Fourier transforms are used. The discrete Fourier transform (DFT) can be expressed by

$$X(f_k) = \frac{1}{N} \sum_{n=0}^{N-1} x(t_n) e^{-j2\pi kn/N} \tag{5.3}$$

and the corresponding inverse discrete Fourier transform (IDFT) is

$$x(t_n) = \sum_{k=0}^{N-1} X(f_k) e^{j2\pi kn/N}. \tag{5.4}$$

There are fast algorithms for calculating DFT and IDFT called the fast Fourier transform (FFT). Characteristic features of the FFT are described in Section 2.2.1.

The standard Fourier transform provides information on the frequency content of a time-domain signal. Since the integral in (5.1) is taken from minus infinity to

plus infinity, the Fourier transform does not give any information on a time period when a given frequency component exists. Thus, the DFT is suitable only for analysis of stationary signals, that is, signals with a time-invariant frequency spectrum. Electrical waveforms in contemporary dynamic power environments, ASD waveforms among them, are non-periodic and non-stationary with sharp edges and transients. Methods of analysis that provide both frequency and time information need to be applied to such signals.

One of the Fourier-based methods for analysis of non-periodic signals is the short-time Fourier transform (STFT) [29]. This method assumes local periodicity of the analyzed waveform and uses a compact support time function by which the signal is multiplied. This compact support time function $w(t)$ is called a window. The continuos STFT is given by

$$X(f,\tau) = \int_{-\infty}^{+\infty} x(t)w(t-\tau)e^{-j2\pi ft}dt. \tag{5.5}$$

The digital version of the SFTF is called a windowed discrete Fourier transform (WDFT) and is expressed by

$$X(f_k,m) = \frac{1}{N}\sum_{n} x(t_n)w(n-m)e^{-j2\pi kn/N}. \tag{5.6}$$

The simplest and most commonly used window type is a rectangle

$$w(n-m) = \begin{cases} 1, & \text{for } 0 \le n-m \le N-1 \\ 0, & \text{otherwise.} \end{cases} \tag{5.7}$$

The WDFT makes it possible to represent a signal in a time-frequency plane. With a fixed window size, the WDFT covers the time-frequency plane with identical rectangles as illustrated in Fig. 5.1(a). Both time and frequency resolution provided by the WDFT is constant at any location of the time-frequency plane. This property of the WDFT is not convenient for analysis of signals that contain a fundamental frequency superimposed with discontinuities or transients. For these signals, fine frequency resolution for low frequency components and fine time resolution for high

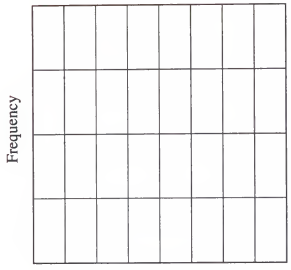

(a)

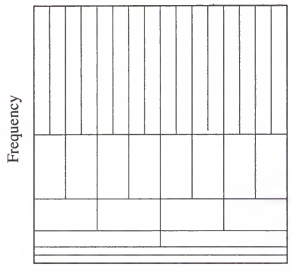

(b)

Figure 5.1: Time-frequency plane coverages. (a) With the short-time Fourier transform. (b) With the wavelet transform.

frequency components are needed. Such a variable time-frequency resolution allows for simultaneous recognition of stationary components and details of fast transients. This type time-frequency plane coverage is shown in Fig. 5.1(b). It can be obtained using the so called wavelet transform.

The wavelet transform of a signal $x(t)$ with respect to the mother wavelet $h(t)$ is given by

$$W_h(a,b) = \frac{1}{\sqrt{a}} \int_{-\infty}^{+\infty} x(t) h^*(\frac{t-b}{a}) dt \tag{5.8}$$

where a is the scale parameter and b is the time-shift parameter. For the wavelet transform invertibility, mother wavelets must be oscillatory, that is, must have a zero average value. Mother wavelets can be non zero for a finite interval of time. Examples of mother wavelets will be given in the next section. The compact-support feature of wavelets, namely, that they exist only for a finite time interval and the possibility of shifting them in the time domain by changing parameter b are analogous to the window in the STFT. The scale parameter a is unique for wavelets. It allows for obtaining fine time resolution [30]. A digital counterpart of the wavelet transform is called the discrete wavelet transform (DWT) and is given by

$$W_h(k,m) = \frac{1}{\sqrt{a_0^k}} \sum_n x(n) h(\frac{m - n a_0^k}{a_0^k}) \tag{5.9}$$

where $a = a_0^k$ and $b = n a_0^k$. The DWT is invertible, that is, it allows for reconstruction of a signal from wavelet coefficients. There are fast algorithms for calculating the DWT.

The wavelet transform can be generalized into a wavelet packet transform. Wavelet packets are certain linear combination of wavelets that preserve orthogonality, smoothness, and localization properties of their parent wavelets. An example of the time-frequency plane coverage using the wavelet packet transform is presented in Fig. 5.2(a). This particular coverage would be convenient for analysis of a signal that contains stationary components in the low-frequency range and at about 3/4

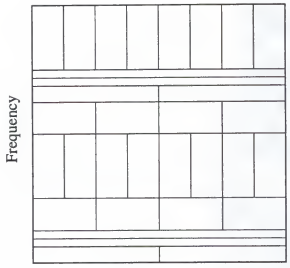

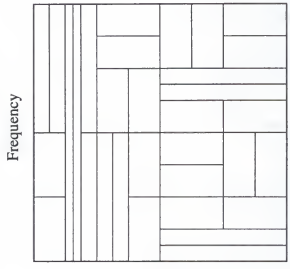

Figure 5.2: Time-frequency plane coverages. (a) With the wavelet packet transform. (b) With the adapted general dyadic transform.

of the Nyquist frequency. Since there is an infinite number of possibilities for the wavelet bases, an adapted wavelet transform can be found that is tailored to the analyzed signal. Fig. 5.2(b) shows an example of an adapted general dyadic coverage of the time-frequency plane. Adapted transforms are used, for instance, in image compression.

5.2 Mother Wavelet Selection

There is an infinite number of possible wavelet families. For every mother wavelet which has a zero average value, there is a corresponding father wavelet with a non-zero average value. Mother and father wavelets are used in compression of images which are two dimensional signals. Mother wavelets are used for analysis of one dimensional signals, e.g., electrical signals. The zero average value property that mother wavelets posses is a condition for the wavelet transform invertibility. Wavelets within each family can be classified by the number of vanishing moments, that is, a set of additional relationships that must be satisfied by wavelet coefficients. Examples of mother wavelets of various shapes and smoothness are presented in Fig. 5.3. The Haar wavelet is the simplest wavelet often used for educational purposes. It is discontinuous. The Daubechies family of wavelets maximizes the smoothness of the father wavelet by maximizing the rate of decay of its Fourier transform. One of the shortest wavelets of the Daubechies family, namely, D6 is depicted in Fig. 5.3. The only one shorter is D4 whereas D2 is equivalent to the Haar wavelet. Mother and father wavelets of the Coiflet have the same number of vanishing moments, six for the case of C3 Coiflet of Fig. 5.3. Symmlets family contains the least asymmetric wavelets of compact support. S6 Symmlet has six vanishing moments.

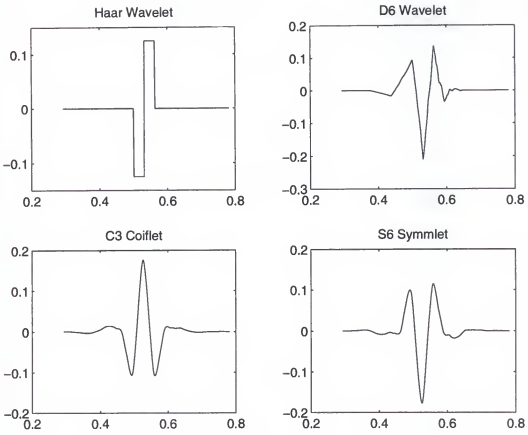

Figure 5.3: Wavelets of compact support with various degrees of smoothness

The infinite number of wavelets poses the problem of selecting an appropriate mother wavelet for a given application. The analyzing mother wavelet should be efficient, that is, a small number of components should represent the most important features of the signal. Adjustable speed drive current and voltage waveforms vary greatly in shape and frequency content. To investigate which mother wavelet is the most efficient for ASD applications, the wavelets of Fig. 5.3 were used for analysis and reconstruction of three selected ASD waveforms: induction motor current, induction motor voltage, and switched-reluctance motor voltage. The waveforms were recreated from wavelet coefficients using 26, 51, and 101 components. The results are summarized in Table 5.1. The error of recreation is defined as the rms value of the difference between recorded and recreated waveforms

$$E_r = \sqrt{\frac{1}{N}\sum_{k=1}^{N}[f(k) - f_r(k)]^2} \tag{5.10}$$

where f is the recorded waveform, f_r is the recreated waveform, T is the recording time, and N is the number of samples. It is the same definition as was used for the recreation of waveforms with FFT in Section 2.2.1. It can be seen from Table 5.1 that no particular mother wavelet yielded the smallest recreation errors for all types of waveforms. Moreover, for a given waveform, the most efficient mother wavelet depended on the number of components used for recreation. In four out of nine investigated recreation cases, the S6 Symmlet turned out to give the smallest error. In another four cases, it was the second most efficient wavelet. Hence, the S6 Symmlet has been selected as the mother wavelet for analysis which results are presented in the next section. To illustrate recreation results produced by selecting various mother wavelets, Figs. 5.4–5.7 show the induction motor voltage waveform recreated using Haar wavelet, D6 wavelet, C3 Coiflet, and S6 Symmlet, respectively. Application of

Table 5.1: Rms Values of Differences Between Recorded Waveforms and Waveforms Recreated with Various Mother Wavelets.

Waveform Type	Induction Motor Current			Induction Motor Voltage			SR Motor Voltage		
Number of Components	26	51	101	26	51	101	26	51	101
Haar Wavelet	0.0798	0.0446	0.0264	0.3154	0.1719	0.0435	0.2860	0.2622	0.2236
D6 Wavelet	0.0541	0.0264	0.0111	0.2587	0.1516	0.0615	0.2957	0.2653	0.2236
C3 Coiflet	0.0589	0.0306	0.0096	0.2714	0.1472	0.0650	0.2909	0.2580	0.2198
S6 Symmlet	0.0575	0.0290	0.0096	0.2661	0.1446	0.0634	0.2881	0.2563	0.2184

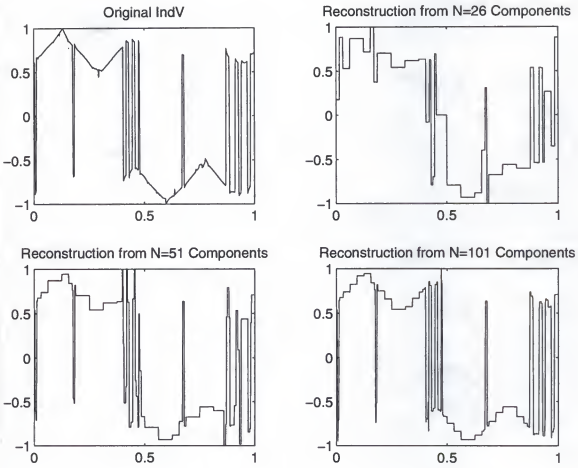

Figure 5.4: Induction motor voltage waveform recreated using Haar wavelet.

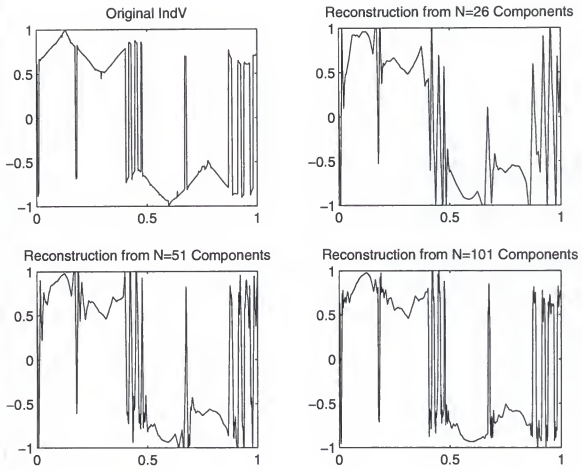

Figure 5.5: Induction motor voltage waveform recreated using D6 wavelet.

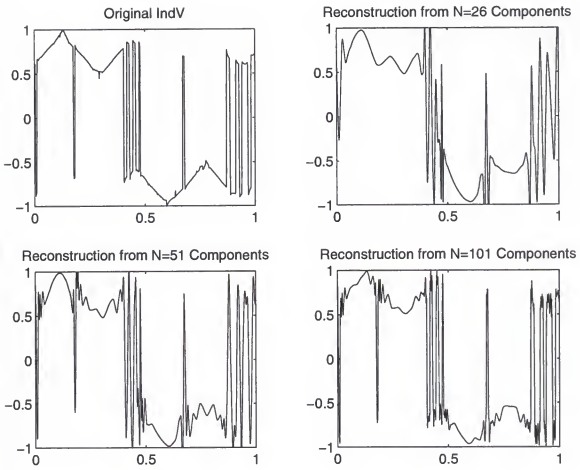

Figure 5.6: Induction motor voltage waveform recreated using C3 Coiflet.

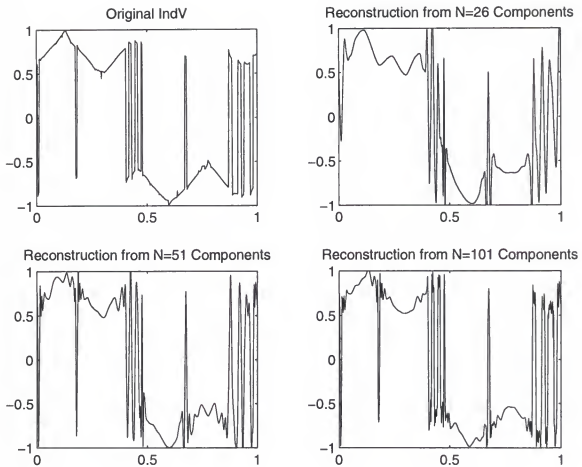

Figure 5.7: Induction motor voltage waveform recreated using S6 Symmlet.

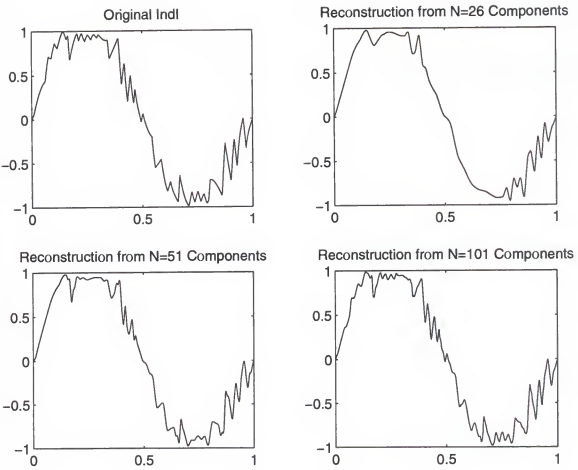

Figure 5.8: Induction motor current waveform recreated using S6 Symmlet.

the most efficient S6 Symmlet to recreation of the induction motor current waveform and the switched-reluctance motor voltage waveform is presented in Figs. 5.8 and 5.9.

5.3 Analysis of Waveforms with DWT

One of the applications of wavelet analysis is in the compression of data. FBI fingerprint archives are stored in this way resulting in hundreds of millions of dollars in memory-cost savings. Data compactness is very important in field-use recording and analyzing instruments that have limited storage capability and that are

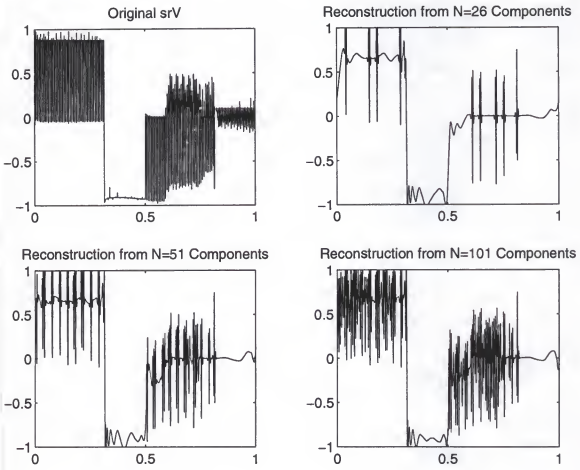

Figure 5.9: Switched-reluctance motor voltage waveform recreated using S6 Symmlet.

Table 5.2: Rms Values of Differences Between Recorded Waveforms and Waveforms Recreated with 51 Components.

Motor	Waveform	FFT	DWT
Induction	Voltage	0.2381	0.1446
	Current	0.0269	0.0290
brushless-dc	Voltage	0.2292	0.1523
	Current	0.0105	0.0091
Switched-reluctance	Voltage	0.2464	0.2563
	Current	0.0046	0.0040

required to send and receive data using modems. Such instruments are predominantly used for adjustable speed drive waveforms. The compression and recreation of ASD waveforms using the DWT has been studied and compared to analogous properties of the FFT. Table 5.2 shows rms values of differences between recorded waveforms and waveforms recreated with 51 most significant components using FFT and DWT S6 Symmlet based analysis. These rms values were calculated using (2.6). It can be seen from Table 5.2 that the DWT yields much smaller recreation errors for the induction motor voltage waveform and for the brushless-dc motor voltage waveform. For other waveforms, the recreation errors are close to each other. What makes the DWT more attractive for data compression than the FFT is a predetermined time-axis location of analyzing wavelets. Thus, only one floating point number representing the amplitude and one integer number representing the order of the wavelet needs to be stored for each component. For the FFT, each component is described by two floating point numbers, the amplitude and the phase, and one integer number providing the order information. Time-domain recreated waveforms using 51 FFT components were shown in Chapter 2. Figs. 5.10–5.12 present the DWT recreation of switched-reluctance motor current waveform, brushless-dc motor voltage waveform, and brushless-dc motor current waveform, respectively. Recreation of other ASD waveforms was shown in the previous section.

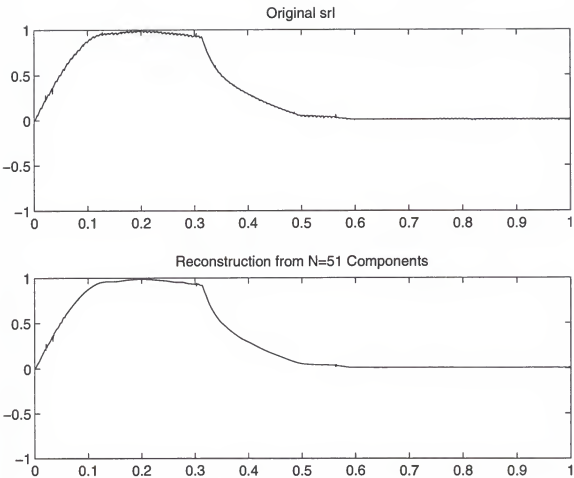

Figure 5.10: Switched-reluctance motor current waveform recreated with 51 DWT components.

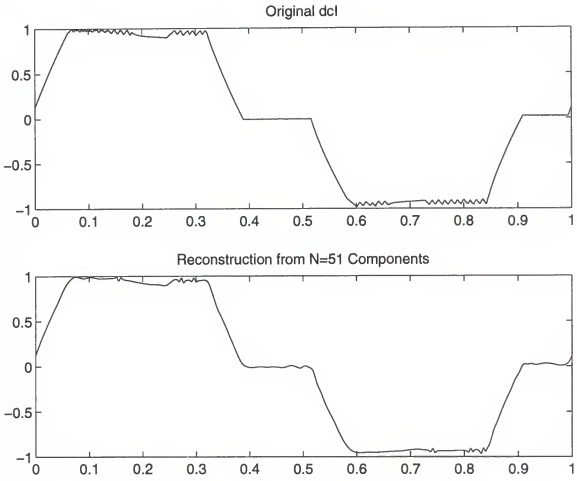

Figure 5.11: Brushless-dc motor current waveform recreated with 51 DWT components.

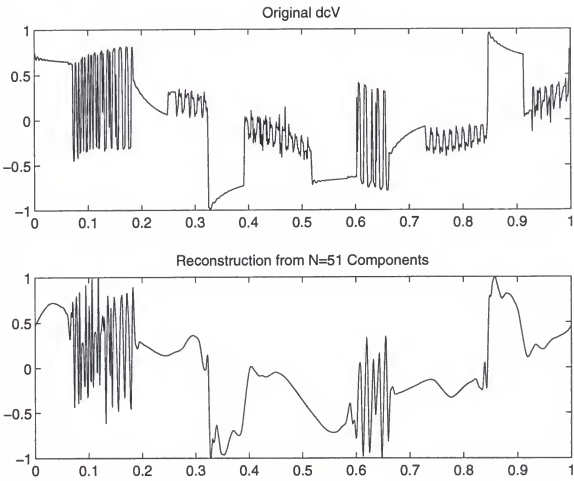

Figure 5.12: Brushless-dc motor voltage waveform recreated with 51 DWT components.

Wavelet analysis can be potentially used in automatic recognition and feature analysis of ASD waveforms. A diagnostic of an ASD's performance would be performed by an expert system or a neural network. Pattern recognition can be done using calculated wavelet coefficients or multiresolution analysis that isolates waveform details at different levels of coarseness. Wavelet coefficients and multiresolution analysis of the induction motor waveforms are presented in Figs. 5.13 and 5.14. Initial results of the wavelet transform application to automatic analysis of power quality disturbances in power systems has been reported [31]–[35]. The methodology presented in these papers can be enhanced towards the ASD waveforms analysis.

In contrast to the Fourier transform, the wavelet analysis is able to provide variable-resolution harmonic content information of an analyzed waveform. Such information is needed for adjustable speed drive designers to optimize the drive performance. PWM controllers can be optimized to reduce current harmonics that decrease motor efficiency. Voltage and current harmonics that produce audible noise and radiate electromagnetic noise can be reduced and filtered if the harmonic order is correctly identified. The wavelet analysis is particularly useful for harmonic analysis of waveforms with transients. ASD's used in servo drives, e.g, in robots, operate mainly in transient states. Another ASD area that could benefit from wavelet analysis is fast estimation of harmonic torque pulsations in inverter-driven induction motors. With current methods of estimation, the low-order harmonics suffer from large errors at low operating frequencies [36]. Figs. 5.15–5.17 show phase plane representations of the induction motor, brushless-dc motor, and switched-reluctance motor voltage waveforms. A S6 Symmlet adapted dyadic base was used for this phase-plane analysis.

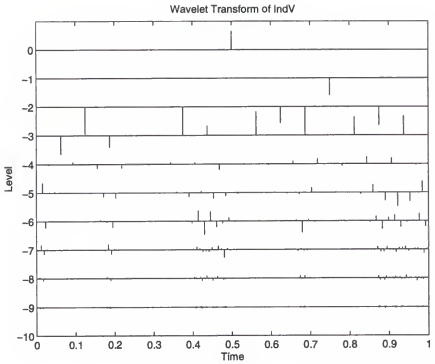

(a)

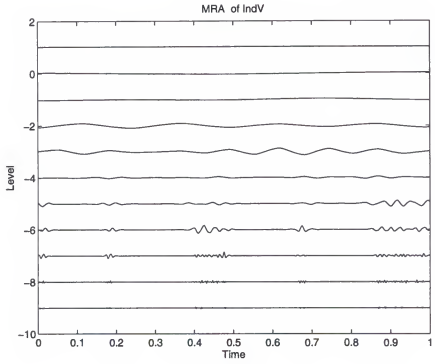

(b)

Figure 5.13: Discrete wavelet transform analysis of induction motor voltage waveform. (a) S6 Symmlet coefficients. (b) Multi-resolution representation.

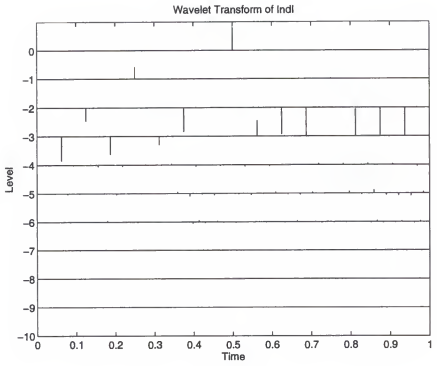

(a)

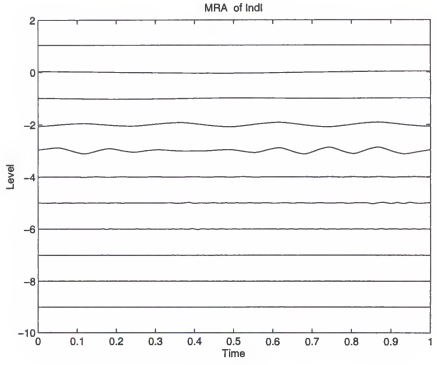

(b)

Figure 5.14: Discrete wavelet transform analysis of induction motor current waveform. (a) S6 Symmlet coefficients. (b) Multi-resolution representation.

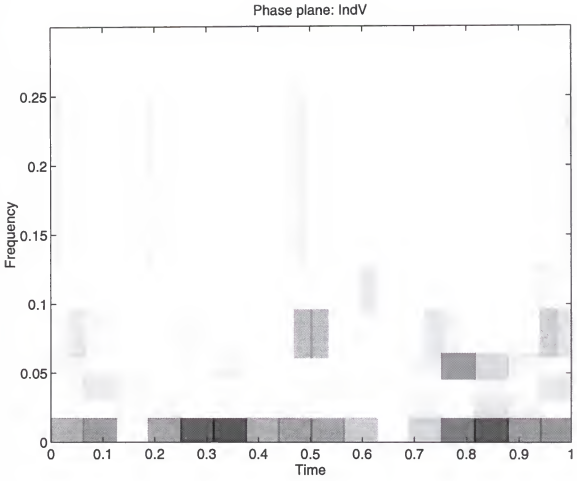

Figure 5.15: Phase plane representation of the induction motor voltage waveform.

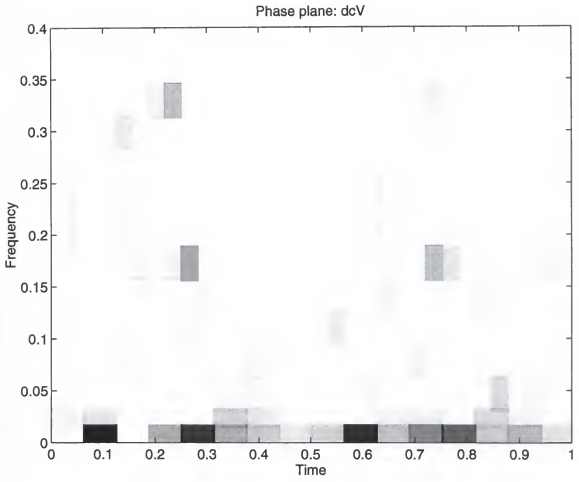

Figure 5.16: Phase plane representation of the brushless-dc motor voltage waveform.

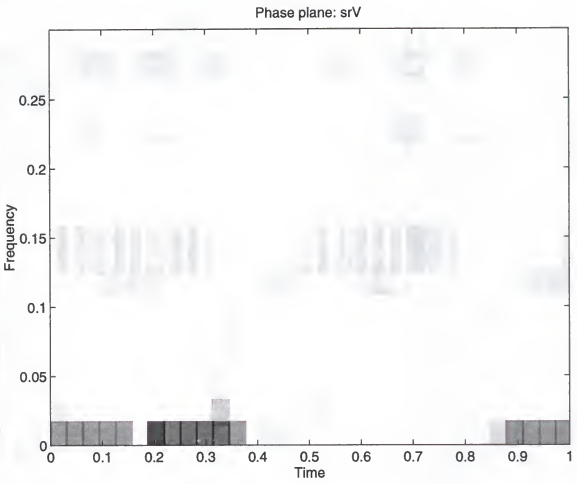

Figure 5.17: Phase plane representation of the switched-reluctance motor voltage waveform.

CHAPTER 6
CONCLUSIONS

6.1 Summary and Conclusions

Voltage and current waveforms that are characteristic for the three main electric drive technologies used in fractional and integral horsepower adjustable speed units, namely, PWM induction, brushless-dc, and switched-reluctance, were recorded. Chapter 2 the gives the results of frequency-domain analysis of the waveforms using the fast Fourier transform (FFT). The harmonic spectrum of PWM inverter-fed brushless-dc and switched-reluctance motors has been presented for the first time. It has been shown that recommended by the IEEE Std 519 monitoring of the first 50 harmonics is sufficient for the adjustable speed drive (ASD) input voltages and currents. The analysis of PWM switched voltages that are supplied by PWM inverters to the motors requires, however, instrumentation with a bandwidth and a harmonic module capable of calculating several hundreds of components.

Three modern power meters were tested for their accuracy under nonsinusoidal conditions. The meters were subjected to waveforms that were characterized in Chapter 2. The meters were extensively tested both under real-world conditions and in a computer-controlled environment. Additionally, the best performing meter was tested for the influence of frequency at unity power factor and the power factor at the fundamental power grid frequency with respect to its accuracy. Results of the tests are presented in Chapter 3. One of the tested meters was able to measure with a satisfactory accuracy input powers to the drives and the input power to the induction motor. All meters failed to measure accurately powers at the input to the brushless-dc and to the switched-reluctance motors. This can be attributed to the

high content of high-frequency harmonics in the voltage spectrum. With a sampling frequency that is only about 5 times higher than substantial harmonics in the instantaneous power waveform, the meters were unable to accurately recreate the power waveform for further processing. Thus, an increase in sampling frequency to a few hundreds of kilohertz is needed to improve the accuracy of power measurements in ASD's applications. Such an increase would also allow for abandoning the equivalent waveform method of measurements that assumes periodicity of the measured waveforms. The real-world ASD waveforms exhibit period by period variations in their rms values around equilibrium points. For efficiency measurements, the measuring channels of multiphase meters should be able to be synchronized independently to either the input or output frequency. In ASD's containing a dc link, the input frequency is the power-grid frequency and the output frequency is adjusted according to the desired rotating speed of a motor. Synchronization circuits should be advanced enough so that synchronization to highly distorted waveforms with multiple or without zero crossings is possible. Solid-state power meters with an increased, as suggested, sampling frequency should be able to achieve 0.2–0.3% accuracy in power measurements of inputs to motors connected to ASD's.

The present industry standards give testing methods that can be followed to obtain the energy efficiency of induction, synchronous, and dc motors under pure sinusoidal or dc conditions which is not the case when ASD's are used. Procedures developed in the course of this research for energy efficiency testing and separation of losses in induction, brushless-dc, and switched-reluctance motor-ASD sets are given in Chapter 4. Various combinations of multi-phase ASD's and multi-phase motors are possible. Therefore, special care should be exercised in selecting an appropriate configuration and in synchronization of power meters. The procedures of Chapter 4 are intended to enhance IEEE and ASHRAE guidelines for motor and ASD testing.

Electrical waveforms in contemporary dynamic power environments are non-periodic and non-stationary with sharp edges and transients. Fourier transform based methods fail to provide appropriate time-frequency resolution for analysis of such signals. To overcome Fourier transform deficiencies, the emerging mathematical tool termed the wavelet transform has been applied to the analysis of ASD waveforms. Results of discrete wavelet transform (DWT) analysis of PWM inverter-fed induction, brushless-dc, and switched-reluctance motor waveforms are presented in Chapter 5. The best mother wavelet for analysis of the recorded waveforms has been selected. Data compression properties of the selected mother wavelet have been compared to those of the FFT. Multilevel feature detection of ASD waveforms using the DWT has been shown. Such a detection scheme can be made a part of quasi-intelligent waveform analyzers. Examples of adaptive time-frequency analysis of PWM voltages have been given. The obtained phase-plane representations can be used in ASD behavior analysis and control algorithm development, especially for transient states.

6.2 Suggestions for Further Research

Power meter and analyzer manufacturers are introducing to the market new models of their products that are intended to meet engineers' and technicians' expectations of power measurement accuracy in more and more sophisticated power electronic equipment applications. The manufacturer claimed accuracy of these new models needs to be tested by an independent laboratory. Close cooperation with manufacturers should be established to provide them with suggestions for their products' improvement, especially in the areas of accuracy, reliability, and user-friendliness.

Practicality of the proposed testing procedures for efficiency tests and separation of losses of ASD-motor sets needs to be verified by the power engineering

community. Feedback from many industrial and academic laboratories must be obtained before the procedures, possibly rewritten and enhanced, may become widely accepted recommended testing practices and, eventually, standards. Similar procedures should be created for other types of ASD's when they enter the market, for instance, synchronous permanent-magnet drives, permanent-magnet reluctance drives, or synchronous-reluctance drives.

The new area of wavelet transform analysis of ASD waveforms offers exciting opportunities for researchers. Wavelet analysis can be used in automatic recognition and feature detection of waveforms. A diagnostic of an ASD's performance would be performed by an expert system or a neural network. Pattern recognition can be done using calculated wavelet coefficients or multiresolution analysis that recognizes waveform details at different levels of coarseness. Adaptive wavelet-based time-frequency decomposition can be applied for efficiency optimization of power converters and control algorithms, particularly in transient states. Developed methods can be transferred to other areas of engineering where non-stationary signals exist.

REFERENCES

[1] D. Jones, "Motion control in global dynamic change," *Control Engineering*, pp. 67-72, Nov. 1995.

[2] D. E. Rice, "A detailed analysis of six-pulse converter harmonic currents," *IEEE Trans. Industry Applications*, Vol. IA-30, pp. 294-304, March/April 1994.

[3] K. D. Hurst and T. G. Habetler, "Sensorless speed measurement using current harmonic spectral estimation in induction machine drives," *IEEE Trans. Power Electron.*, Vol. PE-11, pp. 66-75, Jan. 1996.

[4] J. T. Boys and P. G. Handley, "Spread spectrum switching: low noise modulation technique for PWM inverter drives," *IEE Proc.*, Vol. 139, Pt. B, pp. 252-260, May 1992.

[5] S. R. Bowes, "Novel real-time harmonic minimized PWM control for drives and static power converters," *IEEE Trans. Power Electron.*, Vol. PE-9, pp. 256-262, May 1994.

[6] S. R. Bowes and P. R. Clark, "Regular-sampled harmonic-elimination PWM control of inverter drives," *IEEE Trans. Power Electron.*, Vol. PE-10, pp. 521-531, Sep. 1995.

[7] IEEE Std 519-1992. *IEEE Recommended Practices and Requirements for Harmonic Control in Electric Power Systems.*

[8] A. Domijan, and E. Embriz-Santander, "Measurements of electrical power inputs to variable speed motors and their solid state power converters," *American Society of Heating, Refrigerating and Air-Conditioning Engineers (ASHRAE) Transactions 1993*, Vol. 99, Part I, pp. 241-258.

[9] P. S. Filipski and R. Arseneau, "Behavior of wattmeters and watthour meters under distorted waveform conditions," in *IEEE Tutorial Course, Nonsinusoidal Situations: Effects on the Performance of Meters and Definitions of Power*, Piscataway, NJ: IEEE, 1990, pp. 13-22.

[10] P. S. Filipski and P. W. Labaj, "Evaluation of reactive power meters in the presence of high harmonic distortion," *IEEE Trans. Power Deliv.*, Vol. PWRD-7, pp. 1793-1799, Oct. 1992.

[11] A. Domijan, Jr., E. Embriz-Santander, A. J. Gilani, G. Lamer, C. Stiles, and C. W. Williams, Jr., "Watthour meter accuracy under controlled real-world voltage and current conditions," *IEEE Trans. Power Deliv.*, Vol. 11, No. 1, pp. 64-72, Jan. 1996.

[12] P. S. Filipski, Y. Baghzouz, and M. D. Cox, "Discussion on power definitions contained in the IEEE Dictionary," *IEEE Trans. Power Deliv.*, Vol. PWRD-9, pp. 1237-1244, July 1994.

[13] L. S. Czarnecki, "Considerations on the reactive power in nonsinusoidal situations," *IEEE Trans. Instrumentation and Measurement*, vol. IM-34, pp. 399-404, Sep. 1985.

[14] L. S. Czarnecki, "Comparison of power definitions for circuits with nonsinusoidal waveforms," in *IEEE Tutorial Course, Nonsinusoidal Situations: Effects on the Performance of Meters and Definitions of Power*, Piscataway, NJ: IEEE, 1990, pp. 43-50.

[15] P. S. Filipski and R. Arseneau, "Definition and measurement of apparent power under distorted waveform conditions," in *IEEE Tutorial Course, Nonsinusoidal Situations: Effects on the Performance of Meters and Definitions of Power*, Piscataway, NJ: IEEE, 1990, pp. 37-42.

[16] J. Arrillaga, D. A. Bradley, and P. S. Bodger, *Power System Harmonics*. New York: John Wiley and Sons, 1985, pp. 25–28.

[17] A. A. Girgis and F. M. Ham, "A quantitative study of pitfalls in the FFT", *IEEE Trans. Aerospace and Electronic Systems*, vol. AES–16, pp. 434–439, July 1980.

[18] D. Czarkowski, and A. Domijan, "Harmonic content of PWM adjustable speed drive waveforms – analysis and metering implications," submitted for presentation at the 7th International Conference on Harmonics and Quality of Power, October 16-18, 1996, Las Vegas, Nevada, and publication in the *IEEE Transactions on Power Delivery*.

[19] A. Domijan and D. Czarkowski, "Challenges in electrical power measurements of adjustable speed drives and motors used in HVAC equipment," *ASHRAE Journal*, in press.

[20] D. Czarkowski and A. Domijan, "Performance of electric power meters and analyzers in adjustable speed drive applications," submitted to *ASHRAE Transactions*, 1996.

[21] A. Domijan and E. Embriz-Santander, *Measurements of Electrical Power Inputs to Variable Speed Motors and Their Solid-State Power Converters*, ASHRAE Research Project RP-667 Final Report, 1992.

[22] A. Domijan, D. Czarkowski, A. Abu-aisheh, and E. Embriz-Santander, *Measurements of Electrical Power Inputs to Variable Speed Motors and Their Solid-State Power Converters. Phase II,* ASHRAE Research Project RP-770 Final Report, 1996.

[23] A. Domijan, D. Czarkowski, and J.H. Johnson, "Power measurements of adjustable speed drives," in preparation for submission to the Industry Application Society Meeting and publication in the IAS Transactions (Electric Machines Committee).

[24] E. Embriz-Santander and A. Domijan, "A transducer sensitivity analysis of real power as a function of harmonic magnitudes and angles," submitted for presentation at the 1996 IEEE Summer Meeting, Denver, Co, and publication in the *IEEE Transactions on Power Delivery*, pp. 1-8.

[25] IEEE Std 112-1984. *IEEE Standard Test Procedures for Polyphase Induction Motors and Generators.*

[26] ANSI/IEEE Std 113-1985. *IEEE Guide: Test Procedures for Direct-Current Machines.*

[27] IEEE Std 115-1983. *IEEE Guide: Test Procedures for Synchronous Machines.*

[28] IEEE Std 119-1974. *IEEE Recommended Practice for General Principles of Temperature Measurement as Applied to Electrical Apparatus.*

[29] A. Cohen and J. Kovačević, "Wavelets: the mathematical background," *IEEE Proc.*, Vol. 84, No. 4, pp. 514-522, April 1996.

[30] H. Hess-Nielsen and M. V. Wickerhauser, "Wavelets and time-frequency analysis," *IEEE Proc.*, Vol. 84, No. 4, pp. 523-540, April 1996.

[31] M. P. Collins, W. G. Hurley, and E. Jones, "The application of wavelet theory to power quality diagnostics," *29th Universities Power Engineering Conference*, Galway, Ireland, 1994.

[32] P. F. Ribeiro, "Wavelet transform: an advanced tool for analyzing non-stationary harmonic distortions in power systems," *Proceedings of IEEE ICHPS VI*, Bologna, Italy, pp. 365-369, Sep. 21-23, 1994.

[33] M. P. Collins, W. G. Hurley, and E. Jones, "The application of wavelet theory in an expert system for power quality diagnostics," *30th Universities Power Engineering Conference*, London, Great Britain, 1995.

[34] S. Santoso, E. J. Powers, W. M. Grady, and P. Hofmann, "Power quality assessment via wavelet transform analysis," *IEEE Trans. Power Deliv.*, Vol. PWRD-11, pp. 924-930, Apr. 1996.

[35] D. C. Robertson, O. I. Camps, J. S. Mayer, and W. B. Gish, "Wavelets and electromagnetic power system transients," *IEEE Trans. Power Deliv.*, Vol. PWRD-11, pp. 1050-1058, Apr. 1996.

[36] S. M. Abdulrahman, J. G. Kettleborough, and I. R. Smith, "Fast calculation of harmonic torque pulsations in a VSI/induction motor drive," *IEEE Trans. Industrial Electron.*, Vol. IE-40, pp. 561-569, Dec. 1993.

BIOGRAPHICAL SKETCH

Dariusz Czarkowski was born in Czeladź, Poland. He received the M.S. degree in electronics engineering and the M.S. degree in electrical engineering from the University of Mining and Metallurgy, Cracow, Poland, in 1988 and 1989, respectively. In 1989, he joined the Moszczenica Coal Mining Company and from 1990 he worked as an Instructor at the University of Mining and Metallurgy. From 1991 to 1993, he was a Research Assistant at the Department of Electrical Engineering, Wright State University, Dayton, OH. In 1993, he received the M.S.Egr. degree in electrical engineering from Wright State University. In 1993, he joined Wright State University as an adjunct faculty member. In 1994, Mr. Czarkowski became a Research Associate in the Power Quality and Power Electronics Laboratory at the Department of Electrical and Computer Engineering, University of Florida. Gainesville, FL. His research interests are in the areas of modeling and control of power electronic converters, electric drives, power systems, and modern power devices. Mr. Czarkowski has published ten journal articles (six of them in IEEE Transactions) and numerous conference papers. He coauthored a book "Resonant Power Converters" published by Wiley Interscience in 1995. Mr. Czarkowski is a member of Eta Kappa Nu.

I certify that I have read this study and that in my opinion it conforms to acceptable standards of scholarly presentation and is fully adequate, in scope and quality, as a dissertation for the degree of Doctor of Philosophy.

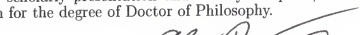

Alexander Domijan, Jr. , Chairman
Associate Professor of Electrical
and Computer Engineering

I certify that I have read this study and that in my opinion it conforms to acceptable standards of scholarly presentation and is fully adequate, in scope and quality, as a dissertation for the degree of Doctor of Philosophy.

Thomas E. Bullock
Professor of Electrical
and Computer Engineering

I certify that I have read this study and that in my opinion it conforms to acceptable standards of scholarly presentation and is fully adequate, in scope and quality, as a dissertation for the degree of Doctor of Philosophy.

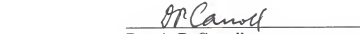

Dennis P. Carroll
Professor of Electrical
and Computer Engineering

I certify that I have read this study and that in my opinion it conforms to acceptable standards of scholarly presentation and is fully adequate, in scope and quality, as a dissertation for the degree of Doctor of Philosophy.

Vladimir A. Rakov
Associate Professor of Electrical
and Computer Engineering

I certify that I have read this study and that in my opinion it conforms to acceptable standards of scholarly presentation and is fully adequate, in scope and quality, as a dissertation for the degree of Doctor of Philosophy.

Barney L. Capehart
Professor of Industrial
and Systems Engineering

This dissertation was submitted to the Graduate Faculty of the College of Engineering and to the Graduate School and was accepted as partial fulfillment of the requirements for the degree of Doctor of Philosophy.

August 1996

Winfred M. Phillips
Dean, College of Engineering

Karen A. Holbrook
Dean, Graduate School